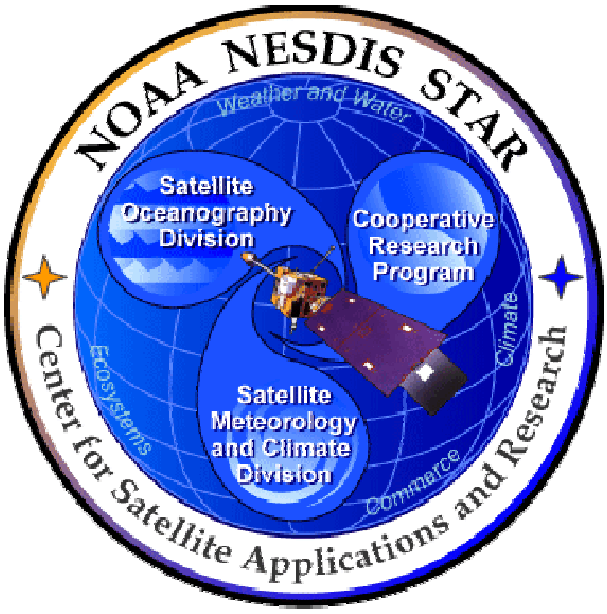


**NOAA NESDIS**
**CENTER for SATELLITE APPLICATIONS and RESEARCH**

# GOES-R Advanced Baseline Imager (ABI) Algorithm Theoretical Basis Document For Land Surface Emissivity

*Jun Li, CIMSS/University of Wisconsin-Madison*
*Zhenglong Li, CIMSS/University of Wisconsin-Madison*
*Xin Jin, CIMSS/University of Wisconsin-Madison*
*Timothy J. Schmit, STAR/NESDIS/NOAA*

*CIMSS emissivity team*
*Algorithm Integration Team*

Version 1.0

July 2010

# TABLE OF CONTENTS

# LIST OF FIGURES

µm from August 2006, and (lower right) operational MODIS/Aqua LSE product for 8.55 µm (collection 4.1) from August 2007. The blank areas are either cloudy or no data.

Figure 9. The scatter plots of 8.7 µm LSE products for (left) SEVIRI, (middle) operational monthly AIRS, and (right) IASI using MODIS/Aqua operational monthly LSE product as reference. The SEVIRI product agrees with MODIS/Aqua product better than both AIRS and IASI.

Figure 10. Same as Figure 8 except for 10.8 µm.

Figure 11. Same as Figure 9 except for 10.8 µm.

Figure 12. Same as Figure 8 except for 12 µm.

Figure 13. Same as Figure 9 except for 12 µm.

Figure 14: The SEVIRI LST products (left) compared with the ECMWF analysis (right) for three time steps: 6 (upper), 12 (middle) and 18 (lower) UTC on August 1 2006. The SEVIRI LSE product better agrees with the actual heating pattern (from east to west).

# LIST OF TABLES

# LIST OF ACRONIMS

| | |
|---|---|
| ABI | Advanced Baseline Imager |
| AIRS | Atmospheric InfraRed Sounder |
| AIT | Algorithm Integration Team |
| ARM | Atmospheric Radiation Measurement |
| ASTER | Advanced Spaceborne Thermal Emission and Reflection Radiometer |
| ATBD | Algorithm Theoretical Basis Document |
| BT | Brightness Temperature |
| C | CONUS |
| CIMSS | Cooperative Institute for Meteorological Satellite Studies |
| CM | Cloud Mask |
| CrIS | Cross-track Infrared Sounder |
| cRTM | Community Radiative Transfer Model |
| CONUS | Continental United States |
| CTP | Cloud Top Pressure |
| ECMWF | European Centre for Medium-Range Weather Forecast |
| EOS | Earth Observing System |
| EUMETSAT | European Meteorological Satellite Agency |
| F&PS | Functional and Performance Specification |
| FOR | Field of Regard |
| FOV | Field of View |
| FVC | Fraction of Vegetation Cover |
| GEO | Geosynchronous |
| GEOCAT | Geostationary Cloud Algorithm Test-bed |
| GFS | Global Forecast System |
| GOES | Geostationary Operational Environmental Satellite |
| HITRAN | High Resolution Transmission |
| IASI | Infrared Atmospheric Sounding Interferometer |
| IR | Infrared |
| JPSS | Joint Polar-orbiting Satellite System |
| LBLRTM | Line-by-line radiative transfer model |
| LEO | Low Earth Orbit |
| LSE | Land Surface Emissivity |
| LST | Land Surface temperature |
| LZA | Local Zenith Angle |
| METOP-A | Meteorological Operational Satellite Programme |

| | |
|---|---|
| MODIS | Moderate Resolution Imaging Spectroradiometer |
| MRD | Mission Requirement Document |
| MSG | Meteosat Second Generation |
| NASA | National Aeronautics and Space Administration |
| NCEP | National Centers for Environmental Prediction |
| NeDR | Noise Equivalent Difference of Radiance |
| NeDT | Noise Equivalent Difference of Temperature |
| NESDIS | National Environmental Satellite, Data, and Information Service |
| NIR | Near Infrared |
| NOAA | National Oceanic and Atmospheric Administration |
| NPOESS | National Polar-Orbiting Operational Environmental Satellite System |
| NPP | NPOESS Preparatory Project |
| NWP | Numerical Weather Prediction |
| OLR | Outgoing Longwave Radiation |
| PFAAST | Pressure-Layer Fast Algorithm for Atmospheric Transmittances |
| PSGS | Perot Systems Government Services, Inc. |
| RAOB | Radiosonde Observation |
| RMSE | Root Mean Square Error |
| RTE | Radiative Transfer Equation |
| RTM | Radiative Transfer Model |
| RTTOV | Rapid Transmissions for TOVs |
| SEVIRI | Spinning Enhanced Visible & Infrared Imager |
| SGP-CART | Southern Great Plains Cloud and Radiation Testbed |
| SSEC | Space Science and Engineering Center |
| STAR | Center for Satellite Applications and Research |
| STD | Standard Deviation |
| TOA | Top of Atmosphere |
| TOVS | TIROS Operational Vertical Sounder |
| TTM | Two-Temperature Method |
| UW | University of Wisconsin |
| VCM | Vegetation Cover Method |
| VIS | Visible |

# ABSTRACT

This document is the Algorithm Theoretical Basis Document (ATBD) for the next generation of Geostationary Operational Environmental Satellite (GOES-R) Land Surface Emissivity (LSE) products. It is a high level description and the physical basis for the physical retrieval of LSE using clear sky infrared (IR) radiances measured by the Advanced Baseline Imager (ABI) to be flown on the GOES-R. The unique feature of geostationary satellite, the time continuity, is utilized to assist and improve the LSE retrieval, in that the LSE is assumed to be invariable within a short period of time while the land surface temperature (LST) is assumed to be variable. This document contains a description of the algorithm, including scientific aspects and practical considerations.

# 1 INTRODUCTION

## 1.1 Purpose of This Document

The land surface emissivity (LSE) algorithm theoretical basis document (ATBD) provides a high level description and the physical basis for the retrieval of LSE using infrared (IR) radiances taken by the Advanced Baseline Imager (ABI) flown on the next generation of Geostationary Operational Environmental Satellite (GOES-R) series of NOAA geostationary meteorological/environmental satellites. The products include LSE, along with land surface temperature (LST), which is simultaneously retrieved from clear sky radiances within $M \times M$ ABI field-of-view (FOV) box area, here one FOV means one pixel. One field-of-regard (FOR) is defined as $M \times M$ FOVs. The ABI LSE product is a new product, which is not provided by the current GOES Sounder.

## 1.2 Who Should Use This Document

The intended user of this document are those interested in understanding the physical basis of the algorithms and how to use the output of this algorithm to optimize the LSE product for a particular application. This document also provides information useful to anyone maintaining, modifying, or improving the original algorithm.

## 1.3 Inside Each Section

This document is broken down into the following main sections.

- **Observing System Overview**: Provides relevant details of the ABI and provides a brief description of the products generated by the algorithm.

- **Algorithm Description**: Provides a detailed description of the LSE algorithm including its physical basis, its input and its output.

- **Test Data Sets and Outputs**: Provides a description of the test data set used to characterize the performance of the algorithm and quality of the data products. It also describes the results from algorithm processing using SEVIRI data.

- **Practical Considerations**: Provides an overview of the issues involving numerical computation, programming and procedures, quality assessment and diagnostics and exception handling.

- **Assumptions and Limitations**: All the assumptions and limitations concerning the algorithm theoretic basis have been described and discussed.

## 1.4 Related Documents

This document currently does not relate to any other document outside of the specifications of the GOES-R Ground Segment Functional and Performance Specification (F&PS) and to the references given throughout.

## 1.5 Revision History

Version 0.0 of this document was created by Dr. Jun Li of Cooperative Institute for Meteorological Satellite Studies (CIMSS) at the UW-Madison and Timothy J. Schmit of Center for Satellite Applications and Research (STAR) of NESDIS, with the intent to accompany the delivery of the version 1.0 algorithms to the GOES-R AWG Algorithm Integration Team (AIT). (July 2008)

Version 0.0 comments/suggestions from N. Nalli (STAR/PSGS) (September 2008)

Version 1.0 was developed by Zhenglong Li, Xin Jin and others to meet 80% ATBD requirement. (July 2010)

# 2 OBSERVING SYSTEM OVERVIEW

## 2.1 Products Generated

The GOES-R Advanced Baseline Imager (ABI) land surface emissivity (LSE) algorithm is responsible for the retrieval of LSE for a field-of-regard (FOR) consisting of $M \times M$ ABI fields-of-view (FOVs). In this document FOR specifically refers to the pixel group for one LSE retrieval. At the time of this writing, $M = 3$ (default) is assumed. The product generation needs brightness temperatures (BTs) from all ABI InfraRed (IR) channels along with numerical weather prediction (NWP) outputs for at least three measurements. The output includes LSE of all window channels along with a bypass product of land surface temperature (LST). Table 1 shows the requirements for LSE products. More requirement information can be found in the GOES-R Mission Requirement Document (MRD) and the Functional and Performance Specification (F&PS).

Table 1. Requirements for GOES-R LSE products .

| Name | User and Priority | Geographic Coverage | Horizontal resolution | Mapping accuracy | Refresh rate | Product measurement precision | Product Extent Qualifier | Conditions Qualifier | Accuracy | Precision[@] |
|---|---|---|---|---|---|---|---|---|---|---|
| LSE | GOES-R | C | 10 km | 5 km | 6 hours | 0.05 | <67 Deg | Clear condition | 0.05 | 0.05 |

[@] pending for approval

The LSE (land surface emissivity) is the relative power of the land surface to emit energy by radiation. It is defined as the ratio of the energy radiated by the land surface to energy radiated by a blackbody at the same temperature. LSE has a spectral variation from as low as 0.6 to 1 depending on the surface materials, soil moisture, vegetation cover and surface roughness.

## 2.2 Instrument characteristics

The next-generation geostationary satellite series will enable many improvements and new capabilities for imager-based products. The ABI (Schmit et al. 2005, see Table 2) on the next-generation GOES-R will improve upon the current GOES imager with more spectral bands, faster imaging, higher spatial resolution, better navigation, and more accurate calibration. The ABI expands from five spectral bands on the current GOES imagers to a total of 16 spectral bands in the visible (VIS), near-infrared (NIR), and IR spectral regions. The coverage rate for full disk scans will increase to at least every 15 min, and the continental U.S. (CONUS) region will be scanned every 5 min. ABI spatial resolution will be 2 km at the sub-point for 10 IR spectral bands, 1 km for select NIR bands, and 0.5 km for the 0.64 μm VIS band (Schmit et al. 2005). It is envisioned that better LSE product will improve selected ABI products, such as sounding and LST products.

Both the current GOES Sounder and Imager have only three IR window channels, which are very sensitive to the surface and are useful for LSE retrieval. ABI, on the other hand, has 5 window spectral bands (3.9, 8.5, 10.35, 11.2 and 12.3 μm), greatly enhancing the ABI's capability to resolve the LSE spectral variation. Studies have shown that the ABI with NWP forecast profiles used as the background, will be able to provide LSE product with quality similar as the operational MODIS products, but with much better temporal resolution.

Table 2. Channel numbers and approximate central wavelengths for the ABI.

| *Channel Number* | *Wavelength (μm)* | *Used in LSE retrieval* | |
|---|---|---|---|
| | | *Regression* | *Physical* |
| 1 | 0.47 | | |
| 2 | 0.64 | | |
| 3 | 0.86 | | |
| 4 | 1.38 | | |
| 5 | 1.61 | | |
| 6 | 2.26 | | |
| 7 | 3.9 | | |
| 8 | 6.15 | ✓ | |
| 9 | 7.0 | ✓ | |
| 10 | 7.4 | ✓ | |
| 11 | 8.5 | ✓ | ✓ |
| 12 | 9.7 | ✓ | |
| 13 | 10.35 | ✓ | ✓ |

| | | | |
|---|---|---|---|
| 14 | 11.2 | ✓ | ✓ |
| 15 | 12.3 | ✓ | ✓ |
| 16 | 13.3 | ✓ | |

# 3 ALGORITHM DESCRIPTION

This section describes the theoretical basis of ABI LSE algorithm and its implementation in Geostationary Cloud Algorithm Test-bed (GEOCAT) using MSG/SEVIRI as proxy.

## 3.1 Algorithm Overview

The current GOES Sounder and Imager (Menzel and Purdom 1994; Menzel et al. 1998) do not provide an operational surface IR emissivity product. However, an emissivity product is very important for other products from GOES-R ABI. Products that require emissivity information include, but are not limited to, temperature and moisture retrievals (Ma et al., 1999; Li et al., 2008), land surface temperature (Becker and Li, 1990; Wan and Dozier, 1996; Yu et al., 2008)), dust and aerosol property retrieval (Zhang et al., 2006; Li et al., 2007), cloud-top pressure (CTP) product (Menzel et al., 1992; Li et al., 2001; Li et al., 2005), Outgoing Longwave Radiation (OLR) and trace gas retrieval (Clerbaux et al., 2003; Ho et al., 2005). In addition, global IR surface emissivity is also very important for the assimilation of IR radiances in numerical weather prediction (NWP) models over land (LeMarshall et al., 2006) and climate modeling and prediction (Jin and Liang, 2006). A global IR surface emissivity product has been developed for the Moderate Resolution Imaging Spectroradiometer (MODIS) (Wan and Li, 1997), and has been used widely in research (Seemann et al., 2008). However, the operational MODIS product provides IR surface emissivity data at only monthly intervals; furthermore, the spectral coverage of the six MODIS IR window bands (3.7, 3.9, 4.0, 8.5, 11.0 and 12.0 μm) are different from that of ABI IR window bands. A monthly global database (Seemann et. al 2008) has been developed based on the MODIS emissivity product and hyperspectral IR emissivity measurements from laboratory measurements. For GOES-R products, such an emissivity database may lack information on temporal variations. Hyperspectral resolution IR sounders onboard the polar orbiting low earth orbit (LEO) satellites, such as the Atmospheric Infrared Sounder (AIRS) (Chahine et al., 2006) onboard the NASA Earth Observing System (EOS) Aqua, the Interferometer Atmospheric Sounding Instrument (IASI) onboard the European Meteorological Operational Satellite Programme (METOP-A), the Cross-track Infrared Sounder (CrIS) on the NPP/JPSS (joint polar-orbiting satellite system), have the capability for retrieving the emissivity spectrum. Recently, an algorithm has been developed for retrieval of hyperspectral IR emissivity spectra from global radiance measurements of advanced sounders (Li et al. 2007; Zhou et al. 2008) onboard LEO satellites such as Aqua and Metop-A (Li and Li 2008). LEO emissivity may be used for geosynchronous (GEO) product since it can be updated routinely and converted to ABI IR bands; however, due to the view angle difference between GEO and LEO, and the orbital gaps of LEO, the application of LEO emissivity to GEO products has some limitations.

Therefore, it is important to develop the emissivity from ABI spectral bands directly so that other ABI products (land surface temperature, dust/aerosol, radiation budget, cloud-top properties, OLR, etc.) have the option to use the ABI emissivity product. The LSE algorithm is developed by the GOES-R AWG emissivity team at the Cooperative Institute for Meteorological Satellite Studies (CIMSS). It is based on the assumption that the LST is temporally variable while the LSE is temporally invariable within a short period of time, i.e. a few hours. GOES-R ABI radiances from multiple time steps are used to retrieve temporally invariable IR LSE and variable LST.

## 3.2 Processing outline

The process initialization gives access to three time steps of ABI IR radiances or BTs, ABI cloud mask (CM), satellite local zenith angle (LZA) and ancillary data (topographic data, land-sea mask, longitude, latitude) for the same location. Only if the pixels or FOR of all the three time steps are labelled as clear (in this 80% version, a conservative scheme is applied which requires all land pixels within the FOR must be clear; plus all pixels within the FOR must be over land) and the satellite zenith angle of all pixels or FOR is below the configurable maximum zenith threshold (set as 67 degree, but in practice the angle is extended to 80°; results with angle larger than 67° will be marked as low quality product in the next version), the LSE retrieval is performed for this FOR.

BTs of all IR channels are read into the LSE algorithm although some of them are not used. NWP forecasts are used as background. The ABI IR radiances are used in two processes. The first one is regression and the second is physical retrieval. In the regression, all IR bands except the 3.9 μm are used in a non-linear regression, which is responsible for supplying the first guesses of LSE and LST as well as other ancillary information needed to drive the radiative transfer model. Although there are multiple methods to determine the first guess, the regressed LST and LSE are used in this 80% version. Three regressions at three time steps will generate three LSE outputs and they are averaged to represent the mean status of LSE first guess during the observations. The NWP products at the current time step are used as additional predictors in the regression with BTs obtained from different time steps due to some technical concerns in GEOCAT. Ideally, NWP products from the three corresponding time steps should be used instead. Although the physical retrieval will be performed only at window channels, which are much less sensitive to the atmospheric conditions, this compromise will inevitably degrade the quality of retrieval. So the total temporal span should be minimized. Currently it is set as 6 hours containing three observations, and the temporal gap between two continuous observations is 3 hours. In the physical algorithm, only the four window channels are used (Table 2), due to the uncertainty of radiative transfer model for channel 3.9 μm, emissivity for this channel is not retrieved. In this version, the algorithm can only support SEVIRI as proxy and the following table is just for reference.

The algorithm relies on spectral and spatial information. The performance of the LSE is therefore sensitive to any imagery artifacts or instrument noise. Calibrated measurements are also critical because the LSE compares the observed radiances to those calculated from a forward radiative transfer model (RTM). The channel specifications are given in

the GOES-R MRD. The land-sea mask is also used as input during the processing step on land pixels. The software has been designed in a very modular way.

Since GEOCAT cannot process CM information of multiple time steps in a single time step and the LSE algorithm requires at least three observations for each channel, it is decided to run the retrieval algorithm four times a day at 0000, 0600, 1200 and 1800. For each run, two ancillary files containing BT and CM information at 3 and 6 hours ago must be prepared in advance. These files are generated by running the cloud mask algorithm only. For example, if we want to run the retrieval for 0600, two files containing BT and CM data for 0000 and 0300 must be pre-processed separately. Since the BT and CM data at 0600 will be stored in the same file containing the retrieval results, we only need to run the cloud mask algorithm for 0900 before the retrieval of 1200.

The whole process includes:

(1) Pre-processing:

- Run cloud mask algorithm twice to generate two ancillary files containing BT and CM information for the third run, i.e. the LSE retrieval algorithm.
- Initialization in the third run: reading of processing options from the configuration file, reading of all coefficient file names, initialisation of RTM, get calibrated ABI IR BTs and associated geographical ancillary data to process, read of ABI CM, etc. Read in the regression coefficient array for non-linear regression to generate the first guess.
- Collect clear pixels within the FOR for retrieval. All pixels within the FOR must be clear for the three time steps and all pixels within the FOR must be on land.
- Averaging the BTs within the FOR to derive the average BT for regression.
- Take collocated forecast temperature and moisture profiles and other 2-D forecast products such as surface air pressure at the third time step as ancillary factors for regression, combining with the BTs from three different time steps, to generate the atmospheric profiles for three different time steps. These profiles will be used as ancillary data in RTM calculation. The regressions also generate LST and LSE for the three time steps. The LST will be used as first guess in the retrieval. Since the LSE are assumed to be unchanged during the past 6 hours, they are averaged as first guess in the following physical retrieval.
- Bias adjustment of ABI BTs. The bias correction coefficients are read from the configuration file and BT correction is made. Since we don't have real data for calibration. This step is not yet to be done. In the 80% version, the bias adjustment for SEVIRI 7.3- and 13.4-um is hardcoded with data from our previous research.

(2) Processing:

- Performing of physical retrieval for LSE and LST in Physical Retrieval Module using the first guess.

- Checking that the retrieved results are between limits and they have physical sense.

(3) Post-processing:
- In this version, quality control has not been done. We need more offline data to evaluate the algorithm.
- Writing of output file.

## 3.3 Algorithm Input

### 3.3.1 Primary Sensor Data

The list below contains the primary sensor data used by the LSE algorithm. The primary sensor data means information that is derived solely from the ABI observations and navigation.

- Calibrated BTs (K) for IR bands 7-16 from $M$ x $M$ (where $M$=3) FOV array, or calibrated BTs (K) for IR bands 7-16 from $M$ x $M$ FOV array for three time steps
- Sensor's local zenith angle (LZA) at the center of each $M$ x $M$ FOV array
- Latitude at the center of each $M$ x $M$ FOV array
- Longitude at the center of each $M$ x $M$ FOV array
- ABI channel use index array
- NeDR (radiance detector noise) array
- ABI CM for each pixel in the $M$ x $M$ FOV array (developed by cloud team) for three time steps

### 3.3.2 Ancillary Data

The following lists and briefly describes the ancillary data required to run the LSE algorithm. Ancillary data means information that is not included in the ABI observations or navigation data.

- **Non-ABI dynamic data**
  - Surface pressure from 6–18 hour forecast from NWP model for the current time step.
  - Surface pressure level index from 6–18 hour forecast from NWP model for the current time step.
  - Temperature profile from 6–18 hour forecast from NWP model for the current time step.
  - Moisture profile from 6–18 hour forecast from NWP model for the current time step.

It is suggested that for CONUS or mesoscale processing, regional NWP output will be used, while global NWP data will be used in full disk processing.

- **Non-ABI static data**

    - The regression coefficient file. This coefficient file contains 81 regression coefficient datasets. Each coefficient dataset corresponds to one LZA ranging from 0 to 80 degrees. The regression coefficient file is an array of 81*110 * (3*L+1+9), where L (=101) is the atmospheric pressure levels used in RTM. In the 80% version, SEVIRI is proxy so the regression coefficient file is an array of 81*108 * (3*L+3+8).

In addition, a clear-sky fast and accurate forward RTM is needed in the iterative physical retrieval process. As of this writing, the LSE algorithm relies on the Pressure-Layer Fast Algorithm for Atmospheric Transmittances (PFAAST) for the radiative transfer calculations, where the profile parameters are represented at a maximum of *L* prescribed pressure levels. PFAAST is based on the line-by-line radiative transfer model (LBLRTM) version 8.4 (Clough and Iacono, 1995) and the high-resolution transmission molecular absorption database-2000 (HITRAN-2000) (Rothman et al., 1992) with updates (aer_hitran_2000_ updat_01.1). In the near future, either the community radiative transfer model (cRTM) or Radiative Transfer for TOVS (RTTOV) will be integrated into the algorithm to replace PFAAST.

## 3.4 Theoretical Description

Land surface IR emissivity is a key parameter for many other ABI products as mentioned in section 3.1. Surface IR emissivity varies with land surface type (according to soil type, land cover, and land use; Snyder et al. 1998; Peres and DaCamara 2005), viewing angle (Francois et al. 1997; McAtee et al. 2003), and time (following changes in the state of the vegetation and weather conditions, such as dew formation, rainfall, or snowfall). Nevertheless, many numerical weather prediction and climate models still use static maps with a limited number of possible emissivity values prescribed per surface type (Jin and Liang 2006; Sherlock 1999; Ogawa and Schmugge 2004). Several methods have been proposed for the retrieval of IR emissivity from remote sensing data. The top of atmosphere (TOA) radiance is a combination of surface emitted radiance (in itself a result of emissivity and surface temperature) and the surface reflection of downward atmospheric flux, which are both absorbed and reemitted by the atmosphere, along with the upward emitted atmospheric radiation. Because of this mixing of surface (emissivity and temperature) and atmospheric signal, the direct retrieval of emissivity is a very difficult problem. Different approaches for solving the direct retrieval of emissivity include the temperature–emissivity separation method followed by the Advanced Spaceborne Thermal Emission and Reflection Radiometer (ASTER) team (Gillespie et al. 1999), the two-temperature method (TTM) (Watson 1992; Faysash and Smith 1999; Faysash and Smith 2000; Peres and DaCamara 2005), the day/night land surface temperature (LST) algorithm applied to MODIS data (Wan and Li 1997), among others (Rodger et al. 2005; Morgan 2005). All of these provide spectral (or channel) emissivity, which would have to be converted into broadband values for numerical model applications. A different approach called the vegetation cover method (VCM) (Peres and

DaCamara 2005; Caselles et al. 1997) consists of the combination of the pixel fraction of vegetation cover (FVC) with a lookup table developed for spectral and broadband emissivities, and assigned to different vegetation and bare-ground types within a land cover classification. The pixel effective emissivity is estimated using information on the proportion of vegetation and exposed surfaces.

All the different approaches for the retrieval of thermal IR emissivity over land surfaces mentioned above have advantages and drawbacks. The choice of a given methodology essentially relies on the sensor characteristics, the required accuracy versus computation time, and the availability of (reliable) atmospheric temperature and humidity profiles. Two methodologies currently pursued by the Satellite Application Facility on Land Surface Analysis (Land SAF, http://landsaf.meteo.pt) (Schmetz et al. 2002; DaCamara 2006): (1) the Land SAF operational scheme consisting of a version of the VCM applied to the Spinning Enhanced Visible and Infrared Imager (SEVIRI) onboard the Meteosat Second Generation (MSG) geostationary satellites and (2) an adaptation of TTM applied to SEVIRI split-window channels.

Taking the advantage of high temporal information, the ABI LSE algorithm is based on the assumption that the surface IR emissivity is temporally invariable while the surface skin temperature is temporally variable within a few hour time periods. Thus, by using ABI window IR radiances from multiple time steps, surface skin temperatures and surface IR emissivity can be derived. Experiments indicate that IR window spectral band radiances from three time steps that have large surface skin temperature contrast are best for success in the ABI surface properties (i.e., surface emissivity and skin temperature) retrieval. The temperature and moisture profiles from a short range forecast model are used for atmospheric correction in the retrieval.

In the version 2.0 algorithm, ABI radiances from three time steps that have 3 hours time difference are used to retrieve three skin temperatures and 4 surface IR emissivities (at ABI IR window bands). Therefore, ABI radiances at the current time step ($T_{current}$) will be used together with that at three hours before ($T_{current} - 3$) and six hours before ($T_{current} - 6$) for the surface skin temperature and emissivity retrieval. In day-2 product, radiances from multiple time steps (more than twice) with 6-hour time periods will be used.

The following describes the theoretical basis for the LSE algorithm. A more detailed and scientific description of this section can be found in Li et al., (2010). Note the following description is written with respect to SEVIRI.

### 3.4.1 Physics of the Problem

Neglecting scattering by the atmosphere, the true clear spectrum of the IR window spectral band radiance exiting the earth-atmosphere system is approximated by the radiative transfer equation (RTE)

$$R = \varepsilon B(T_s)\tau_s - \int_0^p B(T)d\tau(0,p) + (1-\varepsilon)\int_0^p B(T)d\tau^* + R' + e \quad , \qquad (1)$$

where $R$ is the exiting radiance at the top of the atmosphere or SEVIRI IR radiance, $\varepsilon$ is the surface emissivity, $B(T)$ is the Planck function, $\tau(0,p)$ is the atmospheric transmittance from the top to the atmospheric pressure p, subscript s denotes the surface, $\tau^* = \tau_s^2 / \tau$ is the downwelling transmittance, $e$ is forward model uncertainty and $R^{'}$ is the reflected solar radiation, which is ignored in the longwave IR window region. As shown in equation (1), the SEVIRI IR radiance has three major contributions: the surface emission, the upwelling atmosphere emission, and the reflection of the downwelling atmosphere emission by the surface.

The LSE retrieval problem is to solve the land surface emissivity on the right-hand side of equation (1) for the given observations of radiances. Since the LSE is closely coupled with LST to govern the surface emission, the retrieval of LSE must be performed simultaneously with the retrieval of LST. The atmosphere correction is also necessary because of its substantial contribution to the total radiance for the window channels.

## 3.4.2 Mathematical Description

### 3.4.2.1 Radiative transfer equation linearization

Since the inverse problem is non-linear and ill-posed, there are no analytical solutions for the LSE retrieval problem, and regularization is needed. Usually, the first step is to linearize the RTE. Neglecting impacts from ozone and other trace gases, equation (1) could be linearized to the first order as

$$\delta R = K_{T_s} \delta T_s + K_\varepsilon \delta \varepsilon_\nu + \sum K_T \delta T + \sum K_Q \delta \ln Q + e \qquad (2)$$

where $\delta R$ is the radiance perturbation, which is the difference between the observation and the radiative transfer calculation from the first guess, K is the weighting function, defined as $K_x = \frac{\partial R}{\partial x}$, where x is the variable to be retrieved. It shows the sensitivity of the radiance at the top of the atmosphere (TOA) with respect to the change in the variable x. $\sum$ is the sum over different atmospheric layers. Notice the logarithm of the mixing ratio is used instead of the mixing ratio because it has a better linear relationship with the radiance. $e$ in equation (2) contains both forward model uncertainty and observation noise. Equation (2) shows that the radiance perturbation has three components: the LST, the LSE, and the atmosphere (including the temperature and the moisture profiles). Any perturbation in these components results in departure of the calculated radiances from the observed ones.

Figure 1 shows the examination of the first-order linearization approximation using the matchup database. In each panel, only one variable is allowed to have any perturbation (radiative transfer calculation using the first guess instead of the true state), meaning that the radiance perturbation is only caused by that variable. The x-axis represents the calculation from the right-hand side of equation (2), and the y-axis represents the calculation from the left-hand side of equation (2). A perfect linearization approximation would see these two exactly the same.

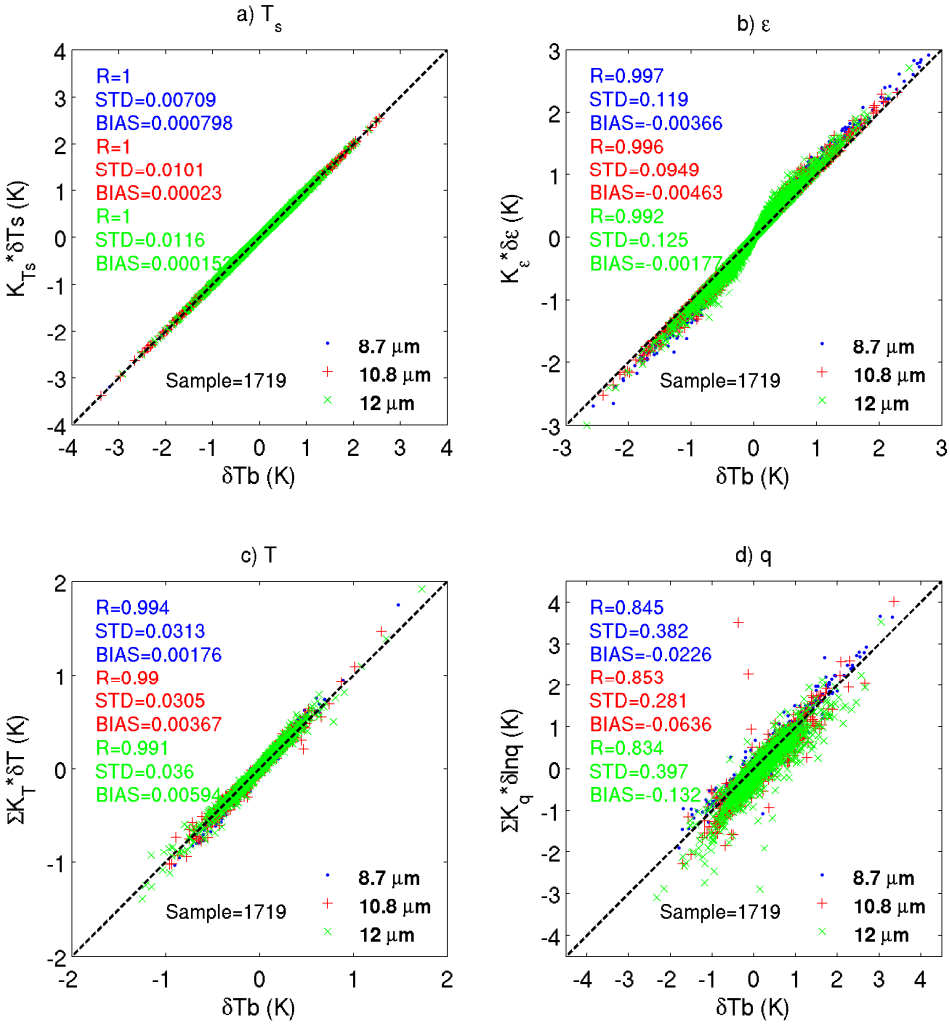


Figure 1. Evaluation of first-order linearization of the radiative equation for SEVIRI channels 7 (8.7 µm), 9 (10.8 µm) and 10 (12 µm) for a) the land surface temperature, b) the surface emissivity, c) the temperature profile, and d) the moisture profile. The x-axis represents the actual Tb differences as observation minus the calculation and the y-axis represents the Tb difference calculated using a first-order linearization approximation. For each panel, only the variable in that panel was perturbed.

All three channels show larger than 0.99 correlation coefficients (R) for LST, LSE and temperature profiles (Figure 1 a, b and c), indicating strong linear relationships. Together with the small STD and bias, it is clear that that radiative transfer equation could be linearized using a first-order linearization approximation with respect to LST, LSE and the temperature profiles. Notice that the large STD of the LSE (0.835 K) at 8.7 µm comes from large perturbations of the 8.7 µm LSE first guess.

However, for the moisture profiles in Figure 1 (d), the first-order linear approximation is not good enough. All three channels have correlation coefficients less than 0.86, and the STDs are larger than 0.28 K, indicating that the first order linear approximation is

insufficient. In fact, better agreements could be reached if a second order expansion for moisture is included (not shown). However, the second order expansion only increases the complexity of equation (2), which makes it more difficult to solve.

#### 3.4.2.2 Atmospheric correction

It is difficult to solve equation (2) with only three window channels. The linearization approximation analysis above shows more complexity with the atmospheric profiles, especially the moisture profiles. It is therefore necessary to simplify equation (2) without introducing significant errors, especially with regard to the atmospheric terms. A simplified equation (2) not only makes it easier to solve for LSE and LST, but also with better retrieval precision.

The simplest way to simplify Equation (2) is to remove the atmospheric contributions (# 3 and 4 terms on the right hand). This removal is equivalent to assuming that the atmospheric states are known and the first guesses of the atmospheric profiles perfectly represent the true state. The first guesses can be either NWP forecast profiles, satellite retrievals or even a climatological background.

In the ABI/SEVIR LSE algorithm, a more advanced atmospheric correction method is utilized; one single variable is used to represent the atmospheric contribution

$$\delta\overline{T}\sum K_T = \sum K_T \delta T + \sum K_Q \delta \ln Q \quad , \tag{3}$$

where $\delta\overline{T}$ is a combination of temperature and moisture error profiles. For each channel, the radiance deviation caused by errors in the atmospheric profiles can be expressed as

$$\delta Tb = \delta\overline{T}\sum K_T \quad . \tag{4}$$

Let $\hat{K}_T = \sum K_T$, the new linearized equation is

$$\delta R = K_{T_s}\delta T_s + K_\varepsilon \delta\varepsilon_\nu + \hat{K}_T\delta\overline{T} + e \quad . \tag{5}$$

This is the equation used to solve LSE and LST along with $\delta\overline{T}$.

#### 3.4.2.3 Time continuity

For a general case, supposing there are N channels, there are N+2 unknowns in Equation (5): 1 LST, N LSE and 1 $\delta\overline{T}$. For a single time, the number of unknowns (N+2) is always larger than the number of equations (N). Therefore equation (5) is under-determined. As a result, it will be difficult to achieve good retrieval precision.

Taking advantage of the high temporal information, the SEVIRI LSE algorithm is based on the assumption that the IR LSE is temporally invariable while LST is temporally variable within a short period of time. Let M be the number of time steps. The total number of equations is $M \times N$. And the number of unknowns is $N + 2M$ (each time step has one LST and one $\delta\overline{T}$). For better retrieval precisions, it is better that the number of equations is equal or larger than the number of unknowns, or

$$M \times N \geq N + 2M \quad . \tag{6}$$

In this study, the number of channels is N=3. The solution of Equation (6) is M ≥ 3; in other words at least three time steps are needed.

The selection of the number of time steps and the time interval between two consecutive time steps is critical. Three factors are considered: the assumption of time continuity, the contrast among different time steps, and cloud contamination. The time span from the first to the last time step cannot be too large, otherwise the assumption of invariable LSE is violated, and the chance for all three observations to be clear is reduced. For better retrieval precision, it is important that there are substantial contrasts between different time steps. Therefore, the time distance between consecutive steps cannot be too small. Experiments with actual SEVIRI observations indicate three time steps with a time range of 3 hours are adequate. Therefore, SEVIRI radiances at the current time step ($T_0$) will be used together with those at three hours before ($T_0 - 3$) and six hours before ($T_0$ - 6) for the LSE and LST retrieval.

#### 3.4.2.4 The inverse algorithm

For three time steps and three channels, there are 9 equations and 9 unknowns. Let

$$\mathbf{Y} = \begin{bmatrix} R_1^1 \\ R_2^1 \\ R_3^1 \\ R_1^2 \\ R_2^2 \\ R_3^2 \\ R_1^3 \\ R_2^3 \\ R_3^3 \end{bmatrix}, \quad \mathbf{X} = \begin{bmatrix} T_s^1 \\ T_s^2 \\ T_s^3 \\ \varepsilon_1 \\ \varepsilon_2 \\ \varepsilon_3 \\ \overline{T}^1 \\ \overline{T}^2 \\ \overline{T}^3 \end{bmatrix}, \text{ and}$$

$$\mathbf{K} = \begin{bmatrix} K_{T_s,1}^1 & 0 & 0 & K_{\varepsilon,1}^1 & 0 & 0 & \hat{K}_{T,1}^1 & 0 & 0 \\ K_{T_s,2}^1 & 0 & 0 & 0 & K_{\varepsilon,2}^1 & 0 & \hat{K}_{T,2}^1 & 0 & 0 \\ K_{T_s,3}^1 & 0 & 0 & 0 & 0 & K_{\varepsilon,3}^1 & \hat{K}_{T,3}^1 & 0 & 0 \\ 0 & K_{T_s,1}^2 & 0 & K_{\varepsilon,1}^2 & 0 & 0 & 0 & \hat{K}_{T,1}^2 & 0 \\ 0 & K_{T_s,2}^2 & 0 & 0 & K_{\varepsilon,2}^2 & 0 & 0 & \hat{K}_{T,2}^2 & 0 \\ 0 & K_{T_s,3}^2 & 0 & 0 & 0 & K_{\varepsilon,3}^2 & 0 & \hat{K}_{T,3}^2 & 0 \\ 0 & 0 & K_{T_s,1}^3 & K_{\varepsilon,1}^3 & 0 & 0 & 0 & 0 & \hat{K}_{T,1}^3 \\ 0 & 0 & K_{T_s,2}^3 & 0 & K_{\varepsilon,2}^3 & 0 & 0 & 0 & \hat{K}_{T,2}^3 \\ 0 & 0 & K_{T_s,3}^3 & 0 & 0 & K_{\varepsilon,3}^3 & 0 & 0 & \hat{K}_{T,3}^3 \end{bmatrix}.$$

Here, the number in superscript denotes the time step, and the number in subscript denotes the channel index.

Equation (5) can be written as

$$\delta \mathbf{Y} = \mathbf{K}\delta \mathbf{X} + \mathbf{e} \ . \quad (7)$$

Here, K is the linear or tangent model of the forward radiative transfer model. It is also called a Jacobian matrix or k-matrix. A simple least square method gives an iterative solution to Equation (7)

$$\delta \mathbf{X}_{n+1} = (\mathbf{K}_n^{'}\mathbf{E}^{-1}\mathbf{K}_n)^{-1}\mathbf{K}_n^{'}\mathbf{E}^{-1}(\delta \mathbf{Y}_n + \mathbf{K}_n \delta \mathbf{X}_n) \ , \quad (8)$$

where $\delta \mathbf{X}_n = \mathbf{X}_n - \mathbf{X}_0$, $\delta \mathbf{Y}_n = \mathbf{Y}^m - \mathbf{Y}(\mathbf{X}_n)$, $\mathbf{K}_n$ is the Jacobian matrix in the nth iteration, $\mathbf{E}$ is the observation error covariance matrix which includes instrument noise and forward model uncertainty. $\mathbf{X}_n$ is the vector of the parameters to be retrieved, $\mathbf{X}_0$ is the initial state or the first guess, $\mathbf{Y}^m$ is the vector of the observed radiances used in the retrieval process, and $\mathbf{Y}(\mathbf{X}_n)$ is the calculated radiances based on the atmospheric and surface state of $\mathbf{X}_n$. For the given first guesses and the satellite observations, the parameters can be retrieved using Equation (8), if the matrix $\mathbf{K}_n^{'}\mathbf{E}^{-1}\mathbf{K}_n$ is invertible.

However, one might find no solution or the solutions may not be realistic because the matrix $\mathbf{K}_n^{'}\mathbf{E}^{-1}\mathbf{K}_n$ is singular or near singular, in which the iteration will be unstable. Any noise in $\delta \mathbf{Y}_n$ will be greatly amplified, and the retrieval will be unrealistic. Therefore, an optimal estimate method is needed to solve equation (7). A general form of the variational solution is to minimize the following cost function (Rodgers 1976; Li et al., 2000)

$$J(\mathbf{X}) = [\mathbf{Y}^m - \mathbf{Y}(\mathbf{X})]^{'}\mathbf{E}^{-1}[\mathbf{Y}^m - \mathbf{Y}(\mathbf{X})] + [\mathbf{X} - \mathbf{X}_0]^{'}\mathbf{H}[\mathbf{X} - \mathbf{X}_0] \ , \quad (9)$$

where $\mathbf{H}$ is the a priori matrix which constrains the solution, and it can be the inverse of the a priori first guess error covariance matrix or another type of matrix. By applying the following Newtonian iteration

$$\mathbf{X}_{n+1} = \mathbf{X}_n + J^{''}(\mathbf{X}_n)^{-1} \bullet J^{'}(\mathbf{X}_n) \ , \quad (10)$$

the following quasi-nonlinear iterative form is obtained

$$\delta \mathbf{X}_{n+1} = (\mathbf{K}_n^{'}\mathbf{E}^{-1}\mathbf{K}_n + \mathbf{H})^{-1}\mathbf{K}_n^{'}\mathbf{E}^{-1}(\delta \mathbf{Y}_n + \mathbf{K}_n \delta \mathbf{X}_n) \ . \quad (11)$$

Compared with the least square method solution in Equation (8), the only difference is that Equation (11) has one extra term $\mathbf{H}$. Physically, this term provides background information, so that the adjustment of the retrieval parameters is made accordingly in the iterations. Mathematically, this term adds extra positive values along the diagonal direction of matrix $\mathbf{K}_n^{'}\mathbf{E}^{-1}\mathbf{K}_n$, decreasing the singularity of it and making the inverse $(\mathbf{K}_n^{'}\mathbf{E}^{-1}\mathbf{K}_n)^{-1}$ possible and stable.

**(a) The first guess ($\mathbf{X}_0$)**

For non-linear ill-posed inverse problems, the quality of the first guess is critical for the retrieval precision. In the simulation study, the 6-hour forecast fields provided by the NCEP (National Centers for Environmental Prediction) GFS at half a degree are used as the temperature and moisture profile first guesses. Each profile is interpolated both in space and time to fit the time and location of the actual satellite observation. The LSE and LST first guesses are randomly generated as described in section 2. When applied to

real data, the LST first guess can be from a regression retrieval using a satellite observation or NWP forecast, while the LSE first guess can be from a regression retrieval using satellite observations or a pre-determined database. In the case of the regression, the averaged emissivities from multiple time steps are used.

**(b) The first guess error covariance matrix**

The first guess error covariance matrix must be consistent with the first guesses. There is no universal covariance matrix suitable for all first guesses. Ideally, the inverse of the first guess error covariance matrix is obtained by inverting the first guess error covariance matrix. Since the first guesses of LSE and LST are randomly generated, the correlative errors are small and negligible, which indicates the off-diagonal elements of the inverse of the error covariance matrix could be set as zero. The diagonal elements are calculated with an LST error of 10 K and LSE error of 10%, 2% and 2% for the three channels, and $\delta\overline{T}$ error of 1 K. Therefore the H matrix is defined as follows:

$$\mathbf{H} = \begin{bmatrix} 0.01 & & & & & & & & \\ & 0.01 & & & & 0 & & & \\ & & 0.01 & & & & & & \\ & & & 100 & & & & & \\ & & & & 2500 & & & & \\ & & & & & 2500 & & & \\ & & & & & & 1 & & \\ & & 0 & & & & & 1 & \\ & & & & & & & & 1 \end{bmatrix}. \quad (12)$$

In the matrix, the 0.01 is derived by 1/(10 * 10), while 100 is derived by 1/(0.1*0.1).

**(c) The observation error covariance matrix**

Normally, matrix $\mathbf{E}$ includes two components: the observation noise and the radiative transfer model uncertainty. The observation noise is estimated based on the instrument's characteristics. It is typically less than 0.15 K for the three window channels. The forward model uncertainty is estimated from the inter-comparison of different radiative transfer models. The uncertainty is assumed to be 0.2 K for the three window channels. Similar to the inverse of the background error covariance matrix, matrix $\mathbf{E}$ is a diagonal matrix. This is equivalent to assuming that there are no correlative errors among the observed radiances and the forward model uncertainties. Matrix $\mathbf{E}$ takes the form

$$\mathbf{E} = \begin{bmatrix} e_{1,1}^2 & & & & & & & & \\ & e_{2,1}^2 & & & & & 0 & & \\ & & e_{3,1}^2 & & & & & & \\ & & & e_{1,2}^2 & & & & & \\ & & & & e_{2,2}^2 & & & & \\ & & & & & e_{3,2}^2 & & & \\ & & & & & & e_{1,3}^2 & & \\ & & 0 & & & & & e_{2,3}^2 & \\ & & & & & & & & e_{3,3}^2 \end{bmatrix}, \quad (13)$$

where $e_{i,j}$ is the combined error from the observation noise and the forward model uncertainty for the $i^{th}$ channel at the $j^{th}$ time step.

**(d) Jacobian matrix**

The Jacobian matrix or k-matrix $\mathbf{K_n}$ (the subscript n denotes the nth iteration in the physical retrieval procedure) describes the change of the radiance at the top of the atmosphere (TOA) with respect to the change in the parameters to be retrieved. It can be calculated by a differential scheme or analytical method (Li et al., 2000). In this study, the latter method is used for computational efficiency.

**(e) Convergence control**

In each iteration, a convergence test is performed based on the increment from the last iteration. Define the mean increment

$$\overline{\mathrm{dX}} = \sqrt{\sum_{i=1}^{m} \delta \mathrm{X}_{n+1}^{i} / m} \ , \quad (14)$$

where $\delta \mathrm{X}_{n+1}^{i}$ is the increment in $n^{th}$ iteration for the $i^{th}$ unknown variable, and $m$ is the number of unknowns. If $\overline{\mathrm{dX}}$ is larger than a given threshold, the iteration continues until the maximum number of iteration is reached.

### 3.4.3 Algorithm Output

The output of the algorithm for each FOR includes:

(1) LSE products in the four window channels (8.5, 10.35, 11.2 and 12.3 μm) for ABI. For SEVIRI, LSE products in three window channels (8.7, 10.8 and 12 μm). Note these LSE products are valid for all the time steps used in the retrieval. The default time steps are three with a time difference of 3 hours.
(2) A by-pass product of LST for all the time steps.

Quality flags (not available for the 80% version delivery):

(3) General Quality Flag: including some general information of each pixel such as space background, latitude range, zenith angle range, missing NWP data, or number of clear pixel, and etc. Please see Table A1 for the detail.
(4) Retrieval Quality Flags: non-convergent iterations, large residual, bad or missing radiance data, etc. The definition of the value assigned to each condition is listed in Tab A2.
(5) Surface Sensitivity Quality Flags: the radiance must show enough sensitivity to the LST and LSE. Our study shows that the LST weighting function of 12 micron must be larger than 0.3 in order for good retrieval. The definition of each value assigned can also be retrieved from Table A1.

Diagnostic/intermediate information:
(6) Number of clear sky pixels in the FOR.
(7) Number of iteration for each retrieval.
(8) Residuals of average BT between observation and calculation after retrieval. Land/Ocean flag. Please see Table A2 for details.

Metadata:
Please refer to Table A3 for the metadata.

# 4 Test Data Sets and Outputs

Since the GOES-R is not launched yet, the ABI LSE algorithm is tested using SEVIRI data. The algorithm is tested using both simulated and observed SEVIRI radiances. More results will be shown later in the 100 % ATBD using simulated ABI radiances.

## 4.1 Input Data Sets

### 4.1.1 The observed SEVIRI radiances as proxy dataset

SEVIRI is a 12-channel imager onboard the Meteosat Second Generation (MSG) (Meteosat 8 and 9). It observes the full disk of the Earth every 15 minutes (Schmetz et al., 2002). Among the 12 SEVIRI channels in Table 3, only the three window channels in thermal IR (TIR) (8.7, 10.8 and 12 μm) are tested. The water vapor (6.2 and 7.3 μm), CO2 (13.4 μm) and ozone (9.7 μm) channels are not sensitive enough to the surface for LSE and LST retrieval. The 3.9 μm channel is excluded due to the difficulty with the radiative transfer calculation from the Sun in the daytime. More information on the SEVIRI can be found in Schmid et al. (2000), Schumann et al. (2002), Aminou et al. (2003), and Schmetz et al. (2002). The algorithm was applied to the SEVIRI observation from August 2006.

Table 3. Spectral channel characteristics of SEVIRI in terms of central, minimum and maximum wavelength of the channels and the main application areas of each channel. The three channels in bold are used for LSE retrieval.

| Channel | Spectral | Characteristics of Spectral | Main observational application |
|---|---|---|---|

| No. | Band (μm) | Band (μm) | | | |
|---|---|---|---|---|---|
| | | λcen | λmin | λmax | |
| 1 | VIS0.6 | 0.635 | 0.56 | 0.71 | Surface, clouds, wind fields |
| 2 | VIS0.8 | 0.81 | 0.74 | 0.88 | Surface, clouds, wind fields |
| 3 | NIR1.6 | 1.64 | 1.50 | 1.78 | Surface, cloud phase |
| 4 | IR3.9 | 3.90 | 3.48 | 4.36 | Surface, clouds, wind fields |
| 5 | WV6.2 | 6.25 | 5.35 | 7.15 | Water vapor, high level clouds, atmospheric instability |
| 6 | WV7.3 | 7.35 | 6.85 | 7.85 | Water vapor, atmospheric instability |
| **7** | **IR8.7** | **8.70** | **8.30** | **9.1** | **Surface, clouds, atmospheric instability** |
| 8 | IR9.7 | 9.66 | 9.38 | 9.94 | Ozone |
| **9** | **IR10.8** | **10.80** | **9.80** | **11.80** | **Surface, clouds, wind fields, atmospheric instability** |
| **10** | **IR12.0** | **12.00** | **11.00** | **13.00** | **Surface, clouds, atmospheric instability** |
| 11 | IR13.4 | 13.40 | 12.40 | 14.40 | Cirrus cloud height, atmospheric instability |
| 12 | HRV | Broadband (about 0.4 – 1.1 μm) | | | Surface, clouds |

### 4.1.2 The simulated SEVIRI radiances

A simulation study using simulated SEVIRI radiances was conducted to help develop, test, diagnosis and improve the algorithm. A match-up dataset (Li et al., 2009, 2010) is used to generate the simulation dataset. This dataset includes:

- The temperature and moisture profiles from radiosonde observations (RAOB) from the U.S. Department of Energy Atmospheric Radiation Measurement (ARM) Program at the Southern Great Plains (SGP) site (Miloshevich et al., 2006) at Lamont, OK (C1, 36°37'N, 97°30'W),

- The GFS 6-hour forecast,

- The laboratory-measured LSE spectrum from the MODIS emissivity library (http://www.icess.ucsb.edu/modis/EMIS/html/em.html) and the ASTER spectral library (Salisbury et al., 1994),

- And the LST measured by the infrared radiometer at the ARM site (Morris et al., 2006).

The time coverage is from August 2006 to August 2009. The sample size for clear skies is 1718.

The ARM RAOBs are preferred to the conventional RAOB because they are more frequent (4 times a day), and have better overall quality (Turner et al., 2003; Li et al.,

2009). The sampling rate is 2 s through the flight. For each sample output, details about time in seconds and a quality flag are provided.

The simulated SEVIRI radiances are calculated using the Pressure-Layer Fast Algorithm for Atmospheric Transmittance (PFAAST) models (Hannon et al., 1996) with the RAOB profiles, the measured LST and the laboratory-measured LSE.

The first guesses of LST and the surface emissivities are generated using

$$x_g = x_t + E(\delta x_t) \tag{15}$$

where $x_g$ is the first guess, $x_t$ is the true parameter, and $E(\delta x_t)$ is a random number with a bias of 0 and a standard deviation (STD) of $\delta x_t$ (10 K for LST; 0.1, 0.02 and 0.02 for emissivities of 8.7, 11 and 12 μm, respectively). The first guesses of LSE are restrained within [0.5 0.99], [0.85 0.99] and [0.9 0.99] for the three channels, respectively. The GFS forecast is used as the first guess for the atmospheric profiles.

## 4.2 Output from LSE algorithm

The primary output from the LSE algorithm is the LSE in three SEVIRI window channels (8.7, 10.8 and 12 μm). These retrieved LSEs are valid for all the given time steps. A bypass product of LST is also returned, for each time step. Figure 2 shows the scatter plots of the three LSE and LST, along with the statistics for the LZA of 0 degree from the simulation study. Note that the noise is added to each channel based on the instrument characteristics and forward model uncertainty. For all four variables, the physical retrieval algorithm successfully brings them closer to the true values. In particular, for LST and LSE at 8.7 μm, the retrievals are significantly better than the first guesses; the root-mean-square (RMS) error for LST is reduced from 10 K to 1.04 K; and the RMS of the 8.7 μm LSE is reduced from 0.087 to 0.018. For the 10.8 and 12 μm LSE, the algorithm is also able to improve the first guesses; the RMS is reduced from 0.018 to less than 0.015. However, the improvements are less significant compared with LST and LSE at 8.7 μm.

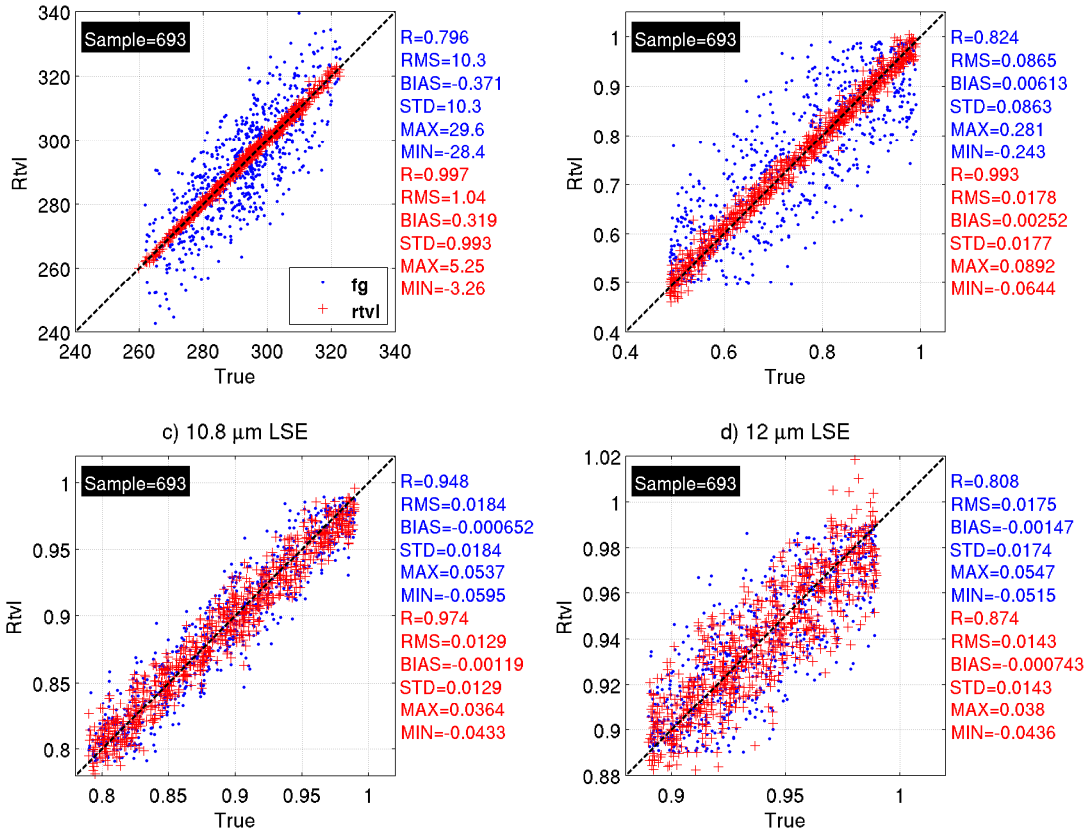


Figure 2. The scatter plots of the retrieval parameters against the true values for a) LST, b) 8.7 µm LSE, c) 10.8 µm LSE and d) 12 µm LSE. Thex-axis represents the true values, and the y-axis represents the retrieved values.

The goal of this study is to develop an algorithm that is less sensitive to: the first guess, the local zenith angle (LZA), radiance noise and radiance bias. It is known that the inverse problem in this study is an ill-posed nonlinear problem, which means the retrieval will be dependent on the quality of the first guesses and observation noise, which in this study include instrument noise and the forward model uncertainty. Figure 3 shows how the quality of the first guess affects the retrieval of LSE and LST. In each panel, only one first guess is allowed to have a different precision. From Figure 3 (a), the retrieval precisions of all four parameters are not affected much by the accuracy of the LST first guess. When the precision of the LST first guess is degraded from 2 K to 10 K, the retrieval precisions for the four parameters are increased by less than 0.01 K, 0.0002, 0.0002, and 0.0002. This result indicates the quality of the LST first guess is not important for the retrieval. Figure 3 (b) shows that the precision of the first guess of the 8.7 µm LSE is not important either. The retrieval precisions for the four parameters are also very weakly affected when the precision of the first guess of the 8.7 µm LSE is increased from 0.02 to 0.1. On the contrary, Figure 3 (c) and 3 (d) show that the retrieval precisions for all four variables are highly affected by the quality of the first guesses of 10.8 and 12 µm LSE. When the precision of the first guess of the 10.8 µm LSE is increased from 0.005 to 0.04, the retrieval precisions are degraded greatly. In particular, for LST the retrieval precision is degraded from 0.96 K to 1.46 K. For the 8.7 µm LSE,

the retrieval precision is also greatly degraded from 0.017 to 0.026. Finally, the 10.8 µm LSE is degraded the most among the three channels; the precision change is 0.013. Comparing Figure 3 (c) and 3(d), the retrieval is slightly less affected by the 12 µm LSE than the 10.8 µm LSE because the 12 µm is more affected by water vapor absorption than the 10.8 µm. The weighting functions of LST and LSE are typically smaller than those for the 10.8 µm, resulting in less sensitivity to the accuracy of the first guess of the 12 µm LSE.

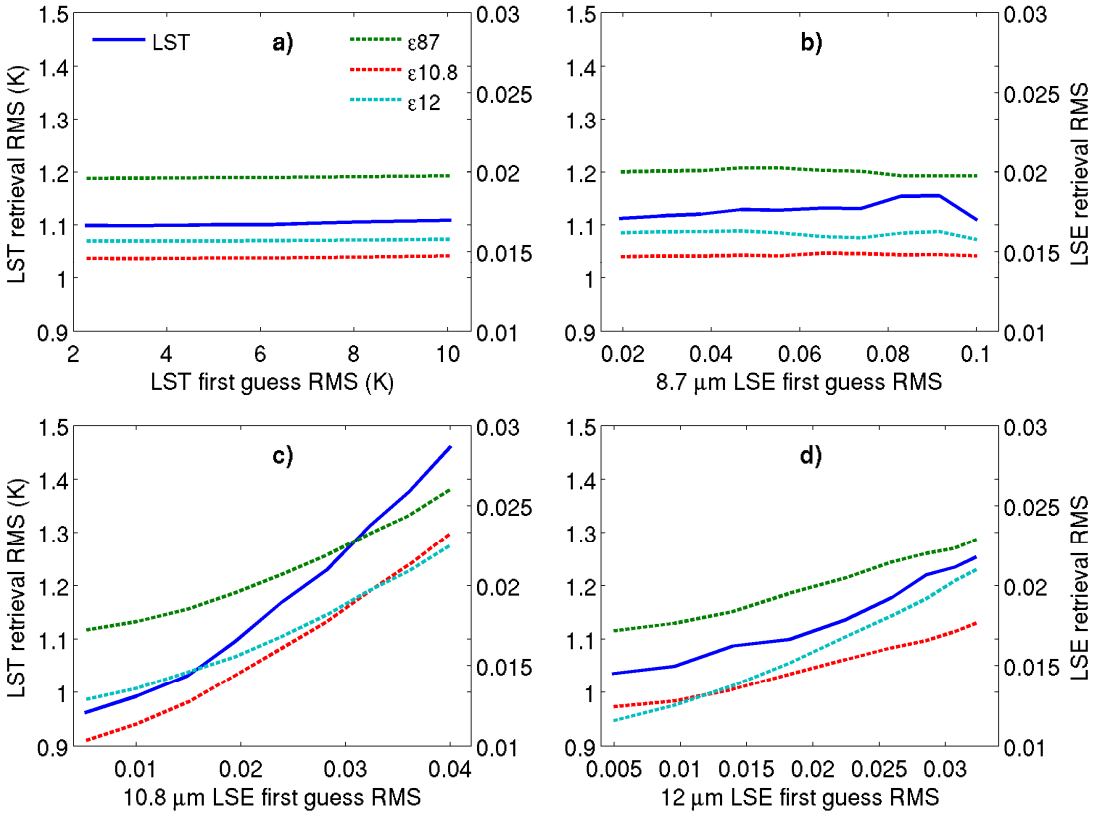


Figure 3. The impacts of the first guesses on the physical retrieval from a) LST, b) 8.7 µm LSE, c) 10.8 µm LSE and d) 12.0 µm LSE. The x-axis represents the RMSE of the first guess. Blue solid lines represent the LST retrieval RMS (the left coordinate). Green, red and cyan dotted lines represent retrieval RMS for 8.7, 10.8 and 12 µm LSE (the right coordinate).

The previous results show that the quality of the first guess is extremely important for the 10.8 and 12 µm LSE, and much less important for the 8.7 µm LSE and LST. These three channels are all in TIR window region, and they are all sensitive to the surface. The question is why the quality of the 10.8 and 12 µm LSE first guesses affect the retrieval much more than that of the 8.7 µm LSE? As shown in Li et al., (2010), the physical reason for the simultaneous use of 10.8 and 12 µm posing more first guess dependency than others is that these two channels observe the surface in a more similar manner than any other two channel combination. As a result, there is more "correlation" between the

two channels than between any other two channels. This makes it difficult to retrieve the two LSE with high accuracy simultaneously.

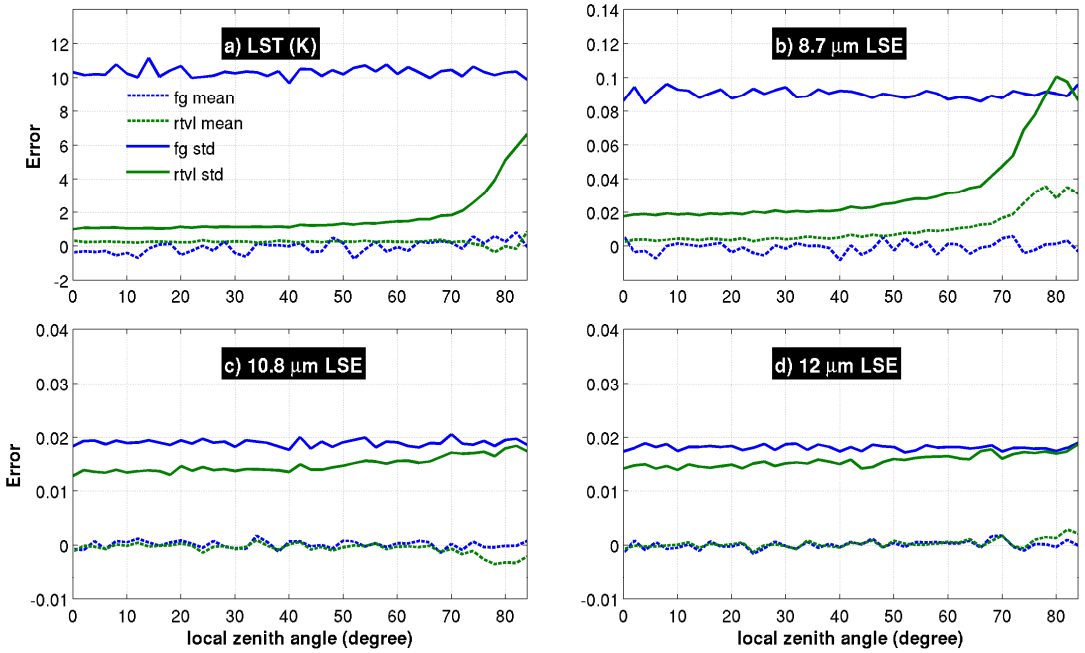


Figure 4. The retrieval accuracy (mean bias error) and precision (STD of error) of a) LST, b) 8.7 μm LSE, c) 10.8 μm LSE and d) 12 μm LSE change with the local zenith angle. The solid lines represent the precision, and the dotted lines represent the accuracy. The blue lines represent the first guesses, and the green lines represent the retrievals.

It is understandable that the retrieval precision is sensitive to the LZA. Usually, as the LZA increases, the retrieval precision decreases. However, it is important that the algorithm works in a wide range of LZAs. Figure 4 shows how the LZA affects the retrieval precision and accuracy. At all LZAs from 0 to 84 degrees, the algorithm is able to improve the first guesses, especially when the LZA is less than 60 degrees. When the LZA is larger than 60 degrees, the precision of LST and LSE at 8.7 μm is degraded quickly and significantly. It is interesting that the precision of LSE at 10.8 and 12 μm is only weakly affected by the increased LZA. This is because fewer constraints are posed on the LST and 8.7 μm LSE in the inverse of the first guess error covariance matrix in Equation (12). As the LZA increases, the channel's sensitivity to the surface decreases. The retrieval becomes more sensitive to the errors in the first guesses and the satellite observations. Retrieval variables with fewer constraints suffer more than variables with strong constraints.

From Figure 4, a cut-off LZA of 67 degrees is recommended; any retrieval with an LZA larger than the cut-off value is considered unreliable. The cut-off of 67 degrees is conservatively chosen for two additional concerns: 1) at large LZAs, the cloud contamination becomes more dominant, as the cloud optical thickness are substantially increased seen by the satellite; and 2) the radiative transfer calculation at large LZAs appears to have worse accuracy and precision.

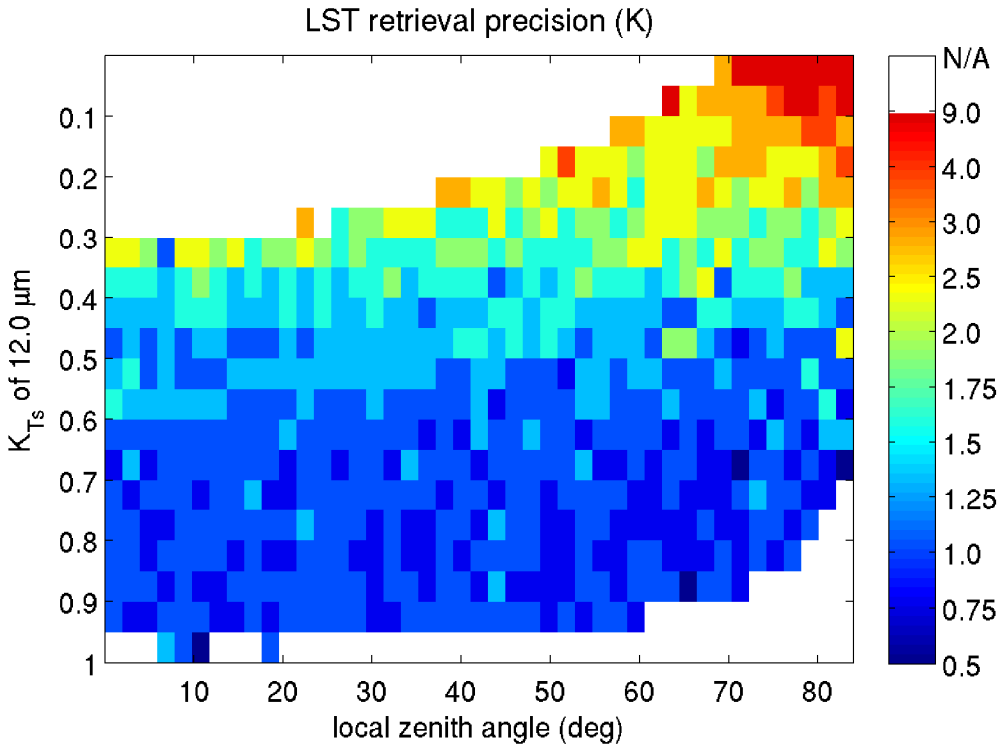

Figure 5. The LST retrieval precision as a function of local zenith angle and 12 µm LST weighting function.

The retrieval with a large LZA has less precision because the weighting functions of LST and LSE statistically decrease with increased LZA. However, even with a large LZA, if the weighting functions are large enough, the retrievals may still be accurate, if there is no cloud contamination and the radiative transfer calculation is reliable (e.g., trained to these angles). Similarly, at low LZA, if the weighting functions are small, the retrievals might be not accurate. Figure 5 shows the retrieval precision of LST as a function of the 12 µm LST weighting function and LZA. The color of each pixel represents the averaged LST retrieval precisions (note the color bar is not linear). The blank pixels are either no retrievals, or the number of retrievals is too small to have statistical meaning. The LST retrieval precisions are better if the 12 µm LST weighting functions are large, regardless of LZA. On the contrary, if the 12 µm LST weighting function is small, the retrieval precisions are worse, no matter how large the LZA is. Clearly, the LST retrieval precision has a better linear relationship with the 12 µm LST weighting function than the LZA. There are two situations in which the 12 µm LST weighting functions are small: 1) the large LZA lowers the 12 µm LST weighting function, and 2) the excessive moisture in the atmosphere greatly attenuates the surface IR emission, reducing the 12 µm LST weighting function. In both situations, the retrieval will have a low precision.

It is critical that the algorithm is not sensitive to the noise in $\delta\mathbf{Y}_n$, including the observation noise and the forward model uncertainty. The observation noise can be estimated from the instrument characteristics, and the forward model uncertainty is 0.2 K

for all three channels. Figure 6 shows how the noise affects the retrievals. Three different levels of noise are added: half (0.5σ+0.1), normal (1.0σ+0.2) and double (2.0σ+0.4). σ denotes the instrument noise. The retrieval precision is only weakly affected by the noise. As the noise increases, the retrieval precisions decrease, but very slowly. When the noise is doubled from half to normal, the changes in retrieval precisions for all four variables are very small. When the noise is doubled from normal to double, the changes are more visible, but still very small. The average LST precision decrease is 0.1 K. And the LSE precision decrease is 0.002, 0.001 and 0.001 for the three channels. These small changes indicate the physical algorithm is only weakly sensitive to the noise. Not shown here is that the retrieval accuracy is not affected by the noise.

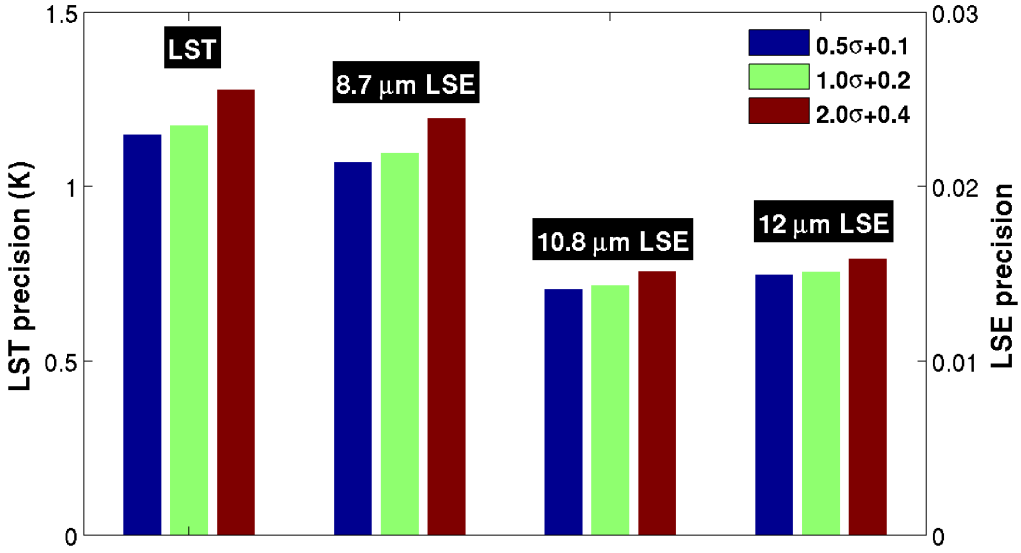


Figure 6. The LST and LSE retrieval precisions affected by noise, including instrumental noise and forward model uncertainty. The left y-axis is for LST, and the right y-axis is for LSE. The blue bars represent half of the noise, the light green color represents normal noise, and the brown bars represent double the noise. The retrieval accuracy is not shown because it is not affected by the noise. σ denotes the instrumental noise.

When applied to real data, the radiance bias is another factor that needs to be addressed. The radiance bias may come from satellite observations due to calibration, dust and cloud contamination, or from the radiative transfer model's failure to accurately simulate water vapor absorption. Dust contamination is a severe problem when applying the method over Africa. Figure 7 shows how the retrievals are affected by the radiance biases. The control run (light green) does not have any radiance biases. Two experimental runs are conducted. In the first one, a radiance bias of -1 K is added to the 8.7 µm Tb to simulate dust contamination. And in the second experiment, a radiance bias of 0.5 K is added to the 12 µm Tb to simulate RT model bias. From Figure 7, the radiance bias in 8.7 µm has little impact on the retrieval of the LST and LSE at 10.8 and 12 µm; the accuracies do not change much from the light green to the blue bars. But it greatly decreases the LSE

accuracy of 8.7 µm from 0.005 to -0.028. In contrast, the radiance bias in 12 µm affects all four variables; the LST is changed by +0.32 K, and LSE is changed by -0.008, -0.007 and 0.008 for the three channels. These changes indicate the physical algorithm is only partially affected by the radiance biases.

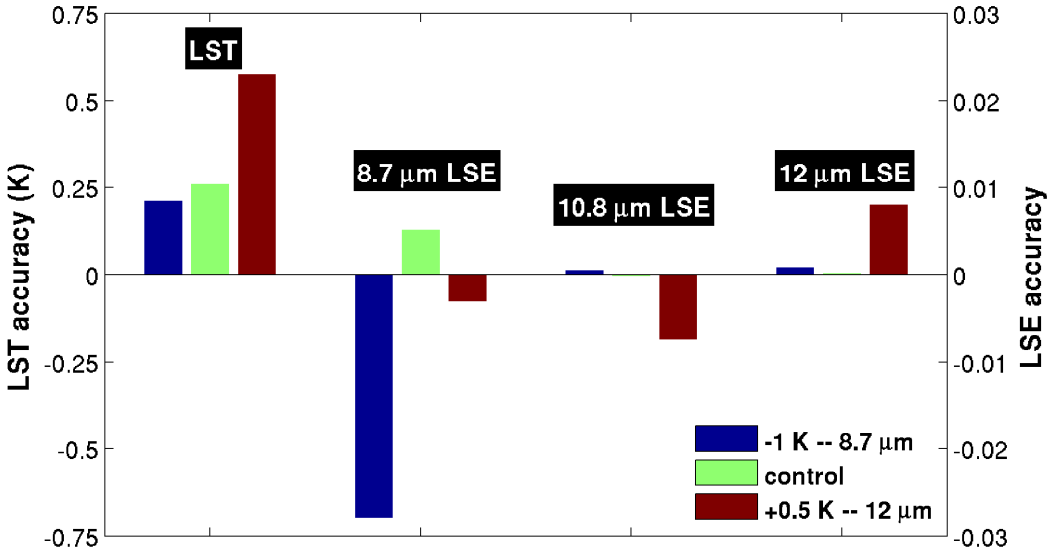


Figure 7. The LST and LSE retrieval accuracy affected by radiance biases. The left y-axis is for LST, and the right y-axis is for LSE. The blue bars represent -1 K for the 8.7 µm radiance bias due to dust contamination. The light green color represents the control run, which has no radiance bias. The brown bars represent +0.5 K for the 12 µm radiance bias from the radiative transfer calculation. The retrieval precision is not shown because it is not affected by the radiance biases.

The SEVIR LSE algorithm is applied to real SEVIRI observations from August 2006. Since there are no enough LSE measurements, no validation has been conducted to quantify the LSE retrieval accuracy and precision. The LSE retrievals have been inter-compared with other LSE products. Figure 8 shows the retrieved SEVIRI LSE imagery for 8.7 µm, along with monthly LSE imagery from IASI, AIRS and MODIS/Aqua. The visual comparison shows that the SEVIRI LSE retrievals have a lot similarity to the operational MODIS/Aqua monthly LSE product, especially geographical distribution. Both the SEVIRI and MODIS/Aqua have much better spatial resolution than the IASI (0.5 degree) and operational AIRS (1 degree) monthly LSE product.

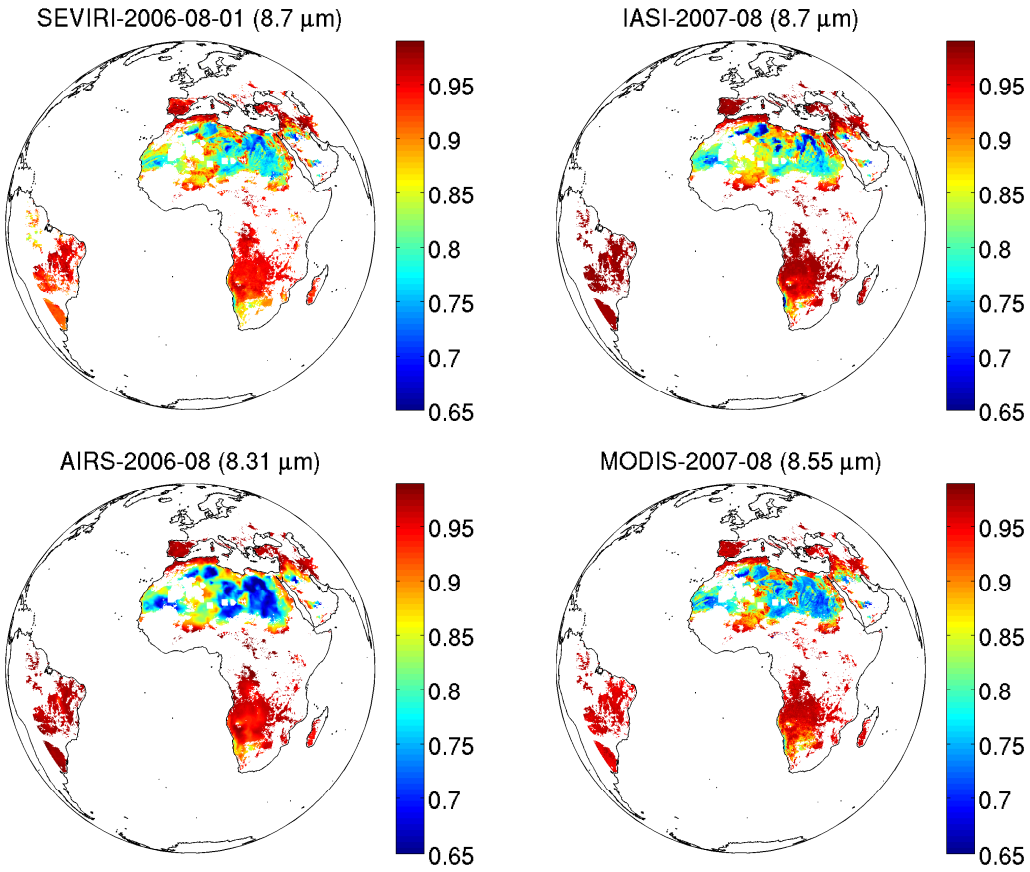


Figure 8. (Top left) the retrieved SEVIRI LSE from August 1 2006 for 8.7 µm, (top right) IASI monthly LSE product for 8.7 µm from August 2007 (after convolved using SEVIRI spectral response function), (lower left) operational AIRS monthly LSE product for 8.7 µm from August 2006, and (lower right) operational MODIS/Aqua LSE product for 8.55 µm (collection 4.1) from August 2007. The blank areas are either cloudy or no data.

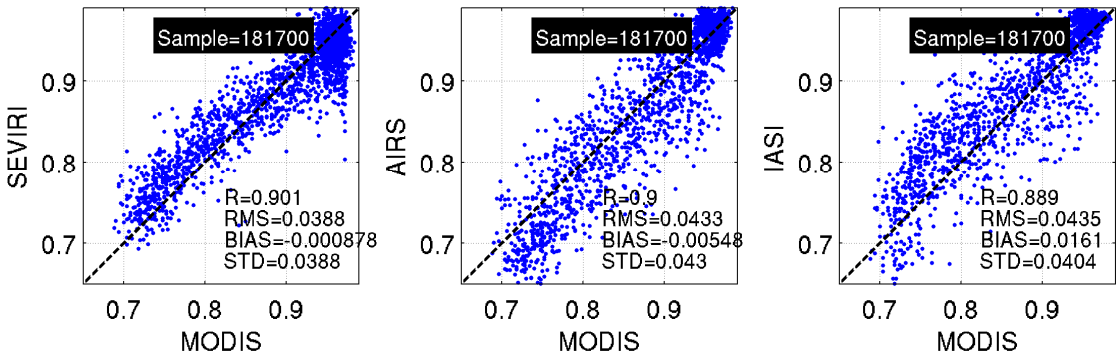


Figure 9. The scatter plots of 8.7 µm LSE products for (left) SEVIRI, (middle) operational monthly AIRS, and (right) IASI using MODIS/Aqua operational monthly LSE product as reference. The SEVIRI product agrees with MODIS/Aqua product better than both AIRS and IASI.

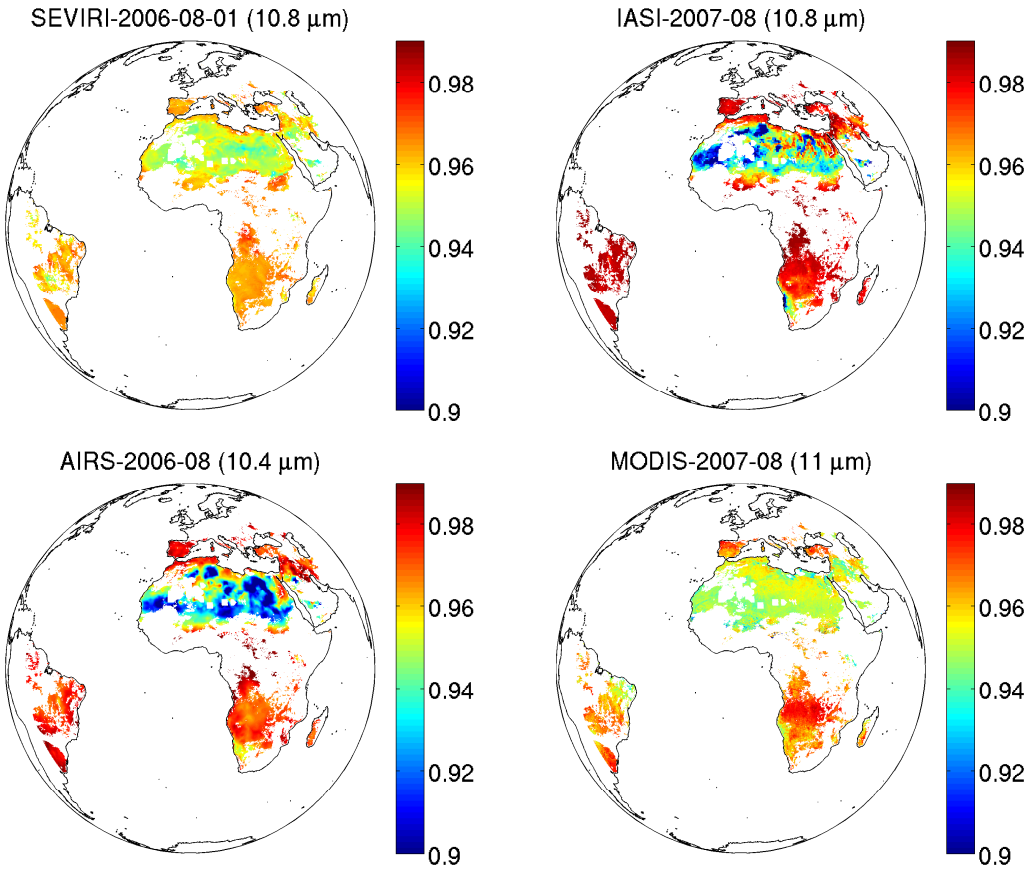


Figure 10. Same as Figure 8 except for 10.8 µm.

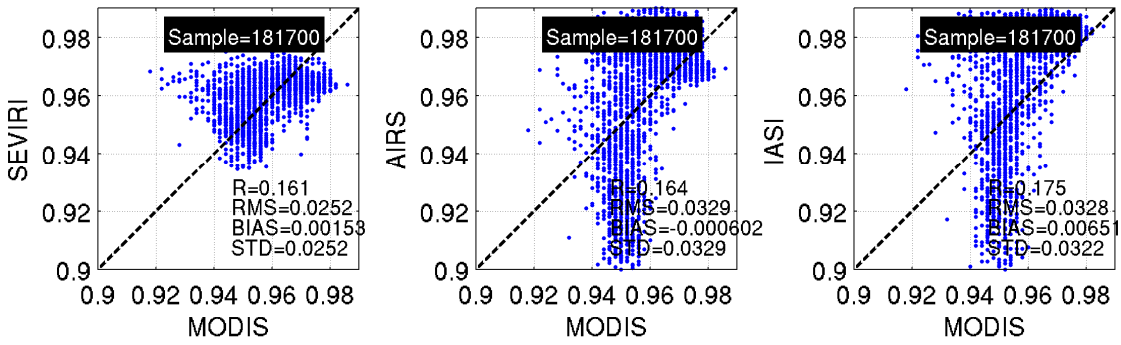


Figure 11. Same as Figure 9 except for 10.8 µm.

According to Li et al., 2010, the operational MODIS/Aqua monthly LSE product has better precisions than both IASI and AIRS. It is used as reference to evaluate the SEVIRI LSE product. Figure 9 shows the scatter plots of the 8.7 µm LSE using MODIS/Aqua operational monthly LSE product (collection 4.1) as reference. Compared with operational AIRS and IASI monthly LSE products, the SEVIRI LSE product has smaller STD (0.0388) and bias (-0.000878), indicating the SEVIRI LSE product has more similarity to the MODIS/Aqua product than AIRS and IASI.

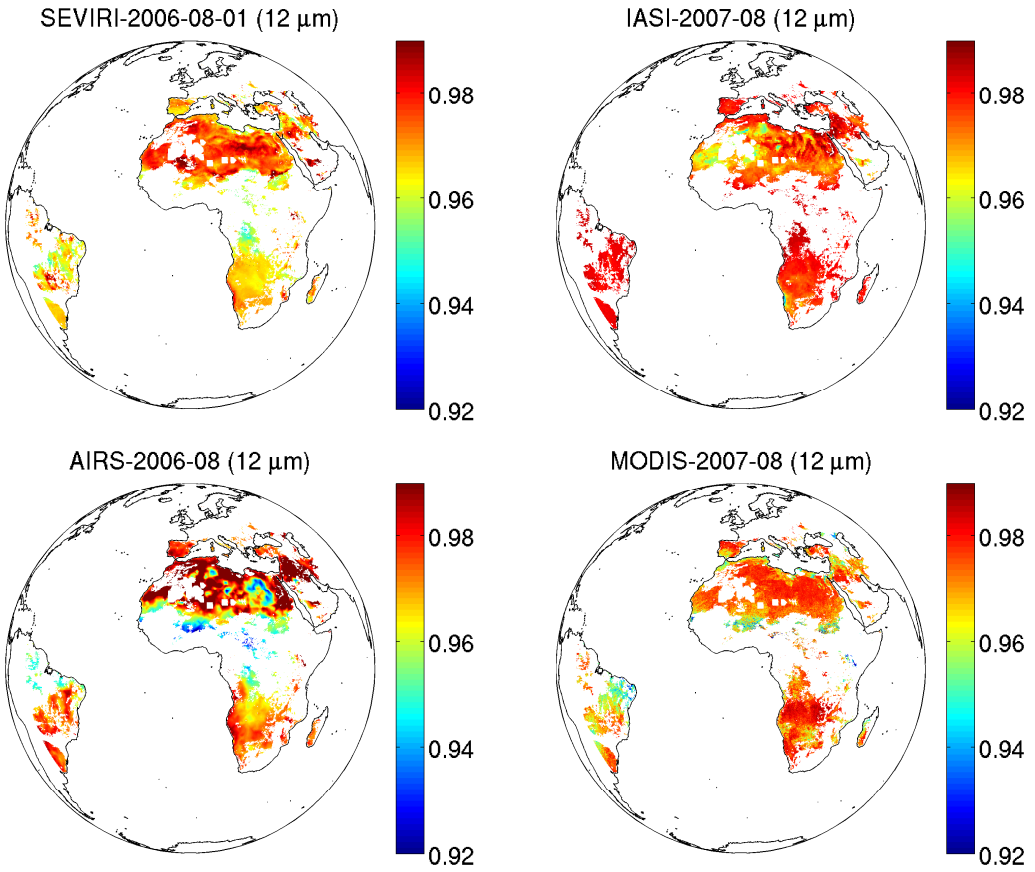


Figure 12. Same as Figure 8 except for 12 µm.

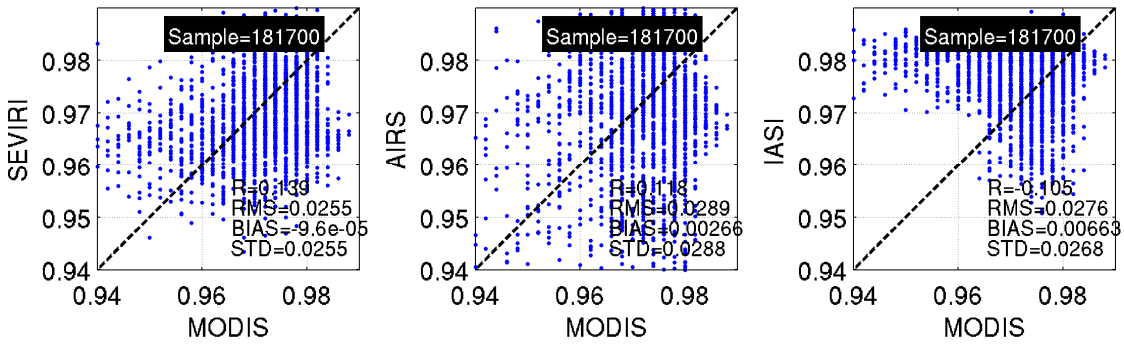


Figure 13. Same as Figure 9 except for 12 µm.

Figures 10 and 12 show the LSE product imagery for 10.8 and 12 µm. Figures 11 and 13 show the scatter plots using MODIS/Aqua as reference for 10.8 and 12 µm. For both 10.8 and 12 µm, the SEVIRI LSE products agree with MODIS/Aqua operational monthly LSE products better than AIRS and IASI.

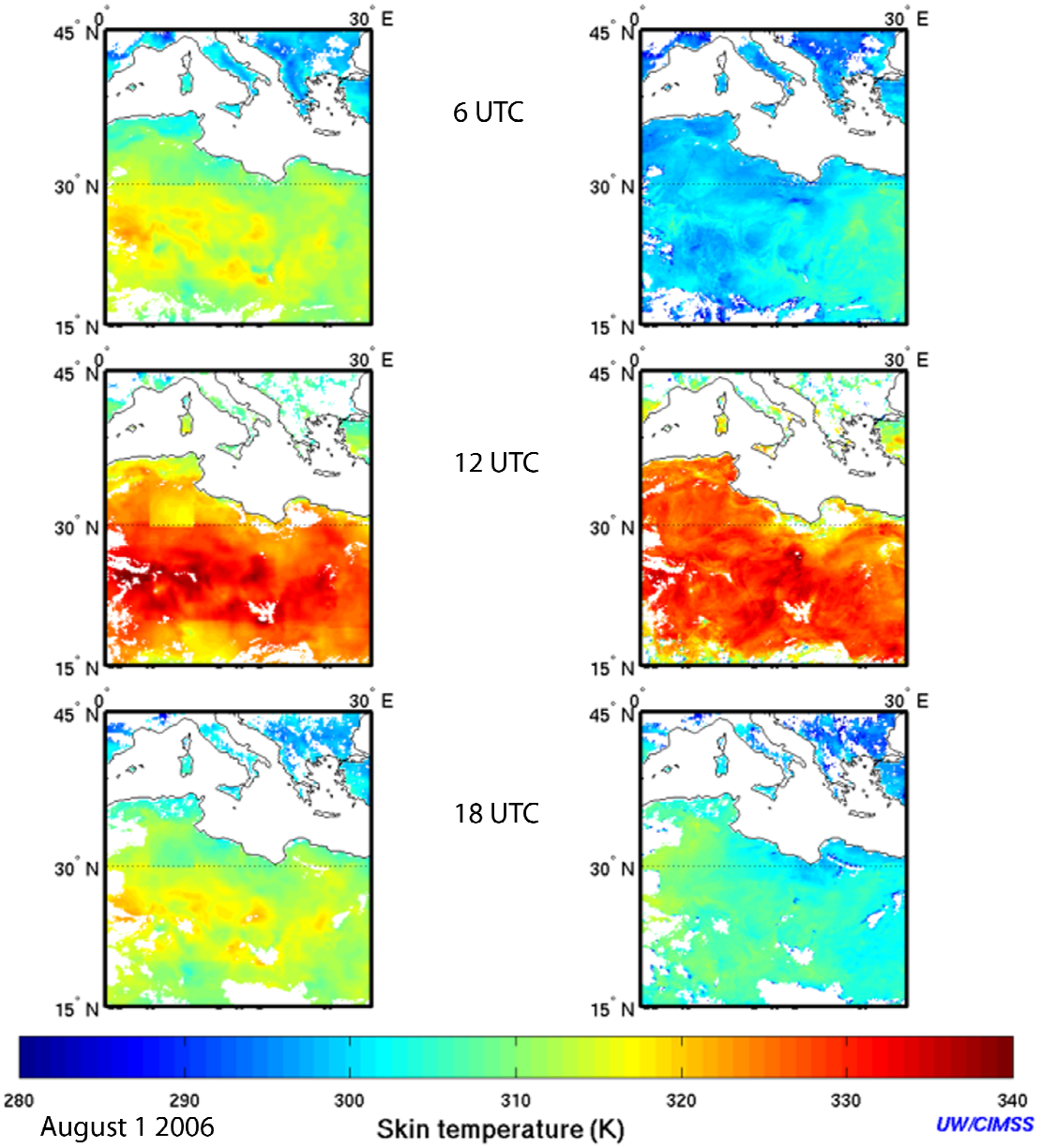


Figure 14. The SEVIRI LST products (left) compared with the ECMWF analysis (right) for three time steps: 6 (upper), 12 (middle) and 18 (lower) UTC on August 1 2006. The SEVIRI LSE product better agrees with the actual heating pattern (from east to west).

An indirect way to qualitatively evaluate SEVIRI LSE product is to compare the by-product of LST retrieved by the SEVIRI LSE algorithm. Since the LSE and LST are simultaneously retrieved from the SEVIRI LSE algorithm, it is expected that the LST product has reasonable value if the LSE is reasonably retrieved. Figure 14 shows the time series of the SEVIRI LST compared with ECMWF analysis over north Africa. In the morning at 6 UTC, the Sun arises from the east, and the SEVIRI LST product successfully reveals that the surface temperature gradient is from the west (low LST) to the east (high LST). The ECMWF analysis, on the other hand, fails to capture that

gradient. At 12 UTC, the Sun is directly overhead. Both the ECMWF and SEVIRI LST show that the heating is all over the place, and the surface temperature gradient is not that much, although the latter shows much better spatial resolution than the former. In the late afternoon at 18 UTC, the Sun moves to the far west. The SEVIRI LST successfully shows the surface temperature gradient is from the east (low LST) to the west (high LST). Again, the ECMWF analysis fails to capture the gradient.

Without LSE measurements, it is difficult to validate the SEVIRI LSE product. According to Li et al. (2010), the LSE precision can be objectively derived using satellite observations. This will be included in the 100 % ATBD.

### 4.2.1 Precision and Accuracy Estimate

The SEVIRI LSE product has not been validated due to the lack of LSE measurements. However, the simulation study with various sensitivity tests shows that the algorithm is stable and efficient. It is expected that the retrieval accuracy and precision are less than 0.03 for the LZA less than 67 degree. Both meet the requirement of 0.05. An objective method, recently developed by Li et al., 2010, will be used to evaluate the LSE precision.

### 4.2.2 Error Budget

Sensitivity studies were conducted to test the algorithm's sensitivity on the first guess, the local zenith angle, the radiance noise and the radiance biases. The simulation study shows that

The algorithm is effective at bringing the LST and LSE at 8.7 µm to the true state, no matter how good the first guesses are.

The algorithm is also able to improve the LSE at 10.8 and 12 µm, although it is more dependent on the quality of the first guesses.

It is found that the retrieval is less sensitive to LZA, but more sensitive to the value of the weighting functions of LSE and LST. As long as the weighting functions are large enough (large sensitivity), the retrieval precisions are good. However, when applying to real data, the retrieval might not be as good as in the simulation when the LZA is large as there might have more radiative transfer uncertainty and cloud contamination in the large LZA. An LZA cut-off of 67 degrees is recommended from the study.

The algorithm is found to be weakly sensitive to the observational random noise, including the observation noise and the forward model uncertainty, while the retrieval is partially sensitive to the radiance biases. The radiance bias in the 8.7 µm from dust contamination only affects the retrieval of the 8.7 µm LSE, while the radiance bias in the 12 µm from the radiative transfer calculation affects the retrieval of LST and all the LSE.

# 5 PRACTICAL CONSIDERATIONS

## 5.1 Numerical Computation Considerations

Both the regression and the physical iterative procedure are mathematically straightforward. The requirement of the computation is not high since there are only 9 variables and 9 equations (for SEVIRI). Besides, the algorithm only runs four times (every 6 hours) a day.

## 5.2 Programming and procedural Considerations

The LSE algorithm requires knowledge of clear mask and NWP forecast information within each FOR. The LSE is implemented sequentially (pre-process, regression followed by iterative physical approach). The LSE is purely a FOR by FOR algorithm. Then it could be parallelized in future version for processing with several CPU. The only task that is not made inside LSE code is spatial interpolation of NWP before retrieval process upon the arrival of new NWP data to avoid repeat the process every slot.

## 5.3 Quality Assessment and Diagnostics

Currently, there is no quality assessment to provide any quality flag of the LSE retrieval. Both the simulation and the application to the observed SEVIRI show that LSE retrievals are reasonable except that some FORs have LSE slightly larger than 1.0 for 12 μm. In the 100 % ATBD, the following procedures will be implemented to diagnose the performance of the LSE.

- Derive BT residuals between observations and calculations with forecast and retrieval.
- The absolute value of LSE should be reasonably less than 1.0.
- The temporal variation of LSE should be small in the surface condition is not changed dramatically.
- The LSE retrieval precision is usually not good when the LST and LSE weighting functions of 12 μm are small.

## 5.4 Exception Handling

Algorithm cannot be run if any of the mandatory IR channels data, ABI CM and NWP forecast is bad or missing. It is required that all of the 3 by 3 FOVs are in clear sky and over land.

## 5.5 Algorithm Validation

### 5.5.1 Pre-launch Validations

The application to both the simulated and the observed SEVIRI radiances shows that the LSE algorithm is effective and efficient. The simulation study shows that the algorithm is particularly effective on retrieving LSE of 8.7 µm and LST, despite of the quality of the first guesses of these two. The algorithm is also effective on retrieving LSE of 10.8 and 12 µm although more dependent on the quality of the first guesses of these two. The inter-comparison to the MODIS/Aqua operational monthly LSE product shows that the SEVIRI LSE agrees with MODIS/Aqua better than both the AIRS and IASI, both of which are hyperspectral instruments.

Recently, an efficient method for quantitatively evaluating the land surface emissivity (LSE) precision using satellite radiance observations is introduced by Li et al. (2010). The LSE Tb deviations, defined as the standard deviations of Tb differences between satellite observations and radiative transfer calculations, can be estimated by minimizing the impacts from land surface temperature (LST) and atmospheric profiles. This is followed by the estimation of LSE precision. This method does not need the true LSE measurements. It only needs ancillary information such as atmospheric profiles and LST, both of which do not require high accuracy and thus can be obtained from an NWP forecast or analysis. The SEVIRI LSE will be compared with AIRS operational products, the MODIS operational products, and the IASI research product. Results will be presented in 100 % ATBD.

### 5.5.2 Post-launch Validations

Similar as the pre-launch validation, the strategy of the post-launch validation mainly consists of two approaches. One, the GOES-R/ABI LSE products will be inter-compared with other LSE products, such as MODIS, AIRS, IASI and CrIS. Second, the objective method developed by Li et al., 2010 will be used to quantitatively evaluate the GOES-R/ABI LSE precisions. If possible, the ABI LSE products will be compared with laboratory measurements.

# 6 Assumptions and Limitations

## 6.1 Performance

The factors impact LSE performance include the inaccuracy of CM, uncertainty of fast RTM, radiance and calibration bias, and imperfect of first guesses of the LSE of the split window channels. The strategies for mitigation include:
(1) For CM improvement, collaborate with cloud team and provide feedback on using their CM product, identify the problematic areas where CM algorithm needs to be improved.
(2) Compare the LSE products retrieved using PFAAST, RTTOV and CRTM. Evaluate the products and choose the one that has the best precision.
(3) For radiance bias, compare the ABI observed radiances to the more accurate hyperspectral observations, such as IASI and AIRS. Derive the radiance bias adjustment coefficients, and these coefficients should be updated routinely.
(4) The first guesses of the split window channels could also be from other LSE databases, such as AIRS, MODIS and IASI. Evaluation will be conducted to determine which one serves the best first guess.

## 6.2 Assumed Sensor Performance

Good ABI radiometric performance is required. The sensitivity study shows that the algorithm is only weakly sensitive to the instrument noise. However, as another source of random noise, the forward model uncertainty might have more impacts on the retrieval. Therefore, an accurate RT model is preferred.

## 6.3 Pre-planned Product Improvements

Here are pre-planned product improvements based on the operational priority and feasibility.

### 6.3.1 Improvement 1: using emissivity database as first guess.

Evaluation will be conducted to determine the better LSE database (from MODIS, AIRS, IASI and UW Baseline Fit) as the first guess.

### 6.3.2 Improvement 2: Radiance bias adjustment

The more accurate hyperspectral radiances from IASI and AIRS will be used to correct SEVIRI/ABI radiances.

### 6.3.3 Improvement 3: Using more sophisticated RT model.

Evaluation will be performed to determine if CRTM or RTTOV is necessary.

### 6.3.4 Improvement 4: Using regional high resolution forecast model

The algorithm benefits from more sophisticated and accurate NWP model. It is believed using regional high resolution NWP model improve the LSE retrieval.

## 6.4 Assumptions

- The single FOV ABI CM is available before the LSE retrieval
- Forecast temperature and moisture profiles, as well as surface pressure are available
- NeDR and calibration for all ABI IR bands are known and reasonably good
- A fast and accurate RTM along with K-Matrix computation are available
- Retrieval is performed on FOR basis
- Spectral response knowledge is stable and known
- ABI satellite position is known
- SSEC quality ABI data with respect to striping, stability, cross-talk, etc.

## 6.5 Limitations

- LSE products are only available over “clear” FORs only (all FOVs within the FOR are clear)
- Effect of emissivity short-term variation is not handled.
- Surface roughness and skin temperature non-homogeneousness are not handled
- Since it is an iterative physical retrieval, computation is relative expensive and increase the width of the FOR could be necessary in large region processing

# 7 REFERENCES


Aminou, D., and coauthors, “Meteosat Second Generation: A comparison of on-ground and on-flight imaging and radiometric performances of SEVIRI on MSG-1,” *Proceedings of ‘The 2003 EUMETSAT Meteorological Satellite Conference’, Weimar, Germany, 29 September – 3 October 2003*, pp. 236–243.

Becker, F., and Z. L. Li (1990), Toward a local split window method over land surface, *Int. J. Remote Sens.*, 11, 369-393.

Caselles, V., E. Valor, C. Coll, and E. Rubio, 1997: Thermal band selection for the PRISM instrument 1. Analysis of emissivity–temperature separation algorithms,” *J. Geophys. Res.*, vol. 102, no. D10, pp. 11 145–11 164.

Chahine, M. T. et al. (2006), AIRS: Improving Weather Forecasting and Providing New Data on Greenhouse Gases, *Bull. Amer. Meteorol. Soc*., *87*, 911-926.

Clerbaux, C., J. Hadji-Lazaro, S. Turquety, G. M´egie, and P.-F. Coheur (2003), Trace gas measurements from infrared satellite for chemistry and climate applications, *Atmos. Chem. Phys. Discuss.*, 3, 2027–2058.

Clough, S. A., and M. J. Iacono (1995), Line-by-line calculations of atmo- spheric fluxes and cooling rates: 2. Applications to carbon dioxide, ozone, methane, nitrous oxide and the halocarbons, J. Geophys. Res., 100, 16,519–16,535, doi:10.1029/95JD01386.

DaCamara, C. C., 2006: The land surface analysis SAF: One year of pre-operational activity, *Proc. EUMETSAT Meteorological SatelliteConf.,* [Online]. Available: http://www.eumetsat.int/Home/Main/Publications/index.htm

Faysash A., and E. A. Smith, 1999: Simultaneous land surface temperature–emissivity retrieval in the infrared split window,” *J. Atmos. Ocean. Technol.*, vol. 16, no. 11, pp. 1673–1689.

Faysash A., and E. A. Smith, 2000: Simultaneous retrieval of diurnal to seasonal surface temperatures and emissivities over SGP ARM-CART site using GOES split window,” *J. Appl. Meteorol.*, vol. 39, no. 7, pp. 971–982.

Francois, C., C. Ottlé, and L. Prevot, 1997: Analytical parameterization of canopy directional emissivity and directional radiance in the thermal infrared. Application on the retrieval of soil and foliage temperatures using two directional measurements, *Int. J. Remote Sens.*, vol. 18, no. 12, pp. 2587–2621.

Gillespie, A., S. Rokugawa, S. Hook, T. Matsunaga, and A. Kahle, 1999:

*Temperature/Emissivity Separation Algorithm Theoretical Basis Document*, Version 2.4. Prepared under NASA Contract NAS5-31372. [Online]. Available: http://eospso.gsfc.nasa.gov/eos_homepage/for_scientists/atbd/docs/ASTER/atbd-ast-05-08.pdf

Hannon, S., L. L. Strow, and W. W. McMillan, 1996: Atmospheric infrared fast transmittance models: A comparison of two approaches. *Proceedings of SPIE*, 2830, 94-105.

Ho, S. P., D. P. Edwards, J. C. Gille, J. M. Chen, D. Ziskin, G. L. Francis, M. N. Deeter, and J. R. Drummond (2005), Estimates of 4.7 Mm surface emissivity and their impact on the retrieval of tropospheric carbon monoxide by Measurements of Pollution in the Troposphere (MOPITT), *J. Geophys. Res.-Atmos.*, 110, D21308, doi:10.1029/2005JD005946.

Jin, M., and S. Liang (2006), Improving Land Surface Emissivity Parameter of Land Surafce Modele in GCM, *J. of Climate*, 19, 2867-2881.

Le Marshall, J., J. Jung, J. Derber, M. Chahine, R. Treadon, S. J. Lord, M. Goldberg, W. Wolf, H. C. Liu, J. Joiner, J. Woollen, R. Todling, P. van Delst, and Y. Tahara (2006), Improving global analysis and forecasting with AIRS, *Bull. Amer. Meteorol. Soc.*, *87*, 891-894.

Li, J., Z. Li, X. Jin, T. J. Schmit, L. Zhou, and M. Goldberg (2010), Land surface emissivity from high temporal resolution geostationary infrared imager radiances – I: Methodology and simulation studies, J. Geophys. Res., submitted.

Li, J., Jinlong Li, Elisabeth Weisz, and D. K. Zhou (2007), Physical retrieval of surface emissivity spectrum from hyperspectral infrared radiances, *Geophysical Research Letters*, 34, L16812, doi:10.1029/2007GL030543.

Li, J., and J. Li, 2008: Derivation of global hyperspectral resolution surface emissivity spectra from advanced infrared sounder radiance measurements, *Geophys. Res. Lett.*, 35, L15807, doi:10.1029/2008GL034559.

Li, J., W. Wolf, W. P. Menzel, W. Zhang, H.-L. Huang, and T. H. Achtor, 2000: Global soundings of the atmosphere from ATOVS measurements: The algorithm and validation, *J. Appl. Meteorol.*, 39: 1248 – 1268.

Li, J., and H.-L. Huang, 1999: Retrieval of atmospheric profiles from satellite sounder measurements by use of the discrepancy principle, *Appl. Optics*, Vol. 38, No. 6, 916-923.

Li, J., P. Zhang, T. J. Schmit, J. Schmetz, and W. P. Menzel (2007), Quantitative monitoring of a Saharan dust event with SEVIRI on Meteosat-8, *International Journal of Remote Sensing*, 28, 2181 – 2186.

Li, J., Menzel, W. P., and A. J. Schreiner (2001), Variational retrieval of cloud parameters from GOES sounder longwave cloudy radiance measurements. *J. Appl. Meteorol.* 40, 312-330.

Li, J., H.-L. Huang, C.-Y. Liu, P. Yang, T. J. Schmit et al. (2005): Retrieval of cloud microphyiscal properties from MODIS and AIRS. *J. Appl. Meteorol.*, 44, 1526 - 1543.

Li, Z., J. Li, X. Jin, T. J. Schmit, E. Borbas, and M. Goldberg (2010), An objective methodology for infrared land surface emissivity evaluation, J. Geophys. Res., submitted.

Li, Z., J. Li, W. P. Menzel, J. P. Nelson, III, T. J. Schmit, E. Weisz, and S. A. Ackerman (2009), Forecasting and nowcasting improvement in cloudy regions with high temporal GOES sounder infrared radiance measurements, J. Geophys. Res., 114, D09216, doi:10.1029/2008JD010596.

Li, Z., J. Li, W. P. Menzel, T. J. Schmit, J. P. Nelson, III, J. Daniels, and S. A. Ackerman (2008), GOES sounding improvement and applications to severe storm nowcasting, *Geophys. Res. Lett.*, 35, L03806, doi:10.1029/2007GL032797.

Ma, X. L., T. J. Schmit, and W. L. Smith (1999), A non-linear physical retrieval algorithm – its application to the GOES-8/9 soundinger, *J. Appl. Meteorol.*, *38*, 501-513.

McAtee, B., A. F. Prata, and M.-J. Lynch, 2003: The behavior of emitted thermal infrared radiation (8–12 $\mu$m) at a semiarid site," *J. Appl. Meteorol.*, vol. 42, no. 8, pp. 1060–1071.

Menzel, W. P., D. P. Wylie, and K. I. Strabala (1992), Seasonal and diurnal changes in cirrus clouds as seen in four years of observations with VAS, *J. Appl. Meteor.*, 31, 370 – 385.

Menzel, W. P., and J. F. W. Purdom, 1994: Introducing GOES-I: The first of a new generation of Geostationary Operational Environmental Satellites. *Bull. Amer. Meteor. Soc.*, **75,** 757–781.

Menzel, W. P., F. C. Holt, T. J. Schmit, R. M. Aune, A. J. Schreiner, G. S. Wade, and D. G. Gray, 1998: Application of GOES-8/9 soundings to weather forecasting and nowcasting. *Bull. Amer. Met. Soc.*, **79**, 2059-2077.

Miloshevich, L. M., H. Voemel, D. N. Whiteman, B. M. Lesht, F. J. Schmidlin, and F. Russo (2006), Absolute accuracy of water vapor measurements from six operational radiosonde types launched during AWEX-G and implications for AIRS validation, J. Geophys. Res., 111, D09S10, doi:10.1029/2005JD006083.

Morgan, J. A., 2005: Bayesian estimation for land surface temperature retrieval: The nuisance of emissivities," *IEEE Trans. Geosci. Remote Sens.*, vol. 43, no. 6, pp. 1279–1288.

Morris, V, C Long, and D Nelson. 2006. "Deployment of an Infrared Thermometer Network at the Atmospheric Radiation Measurement Program Southern Great Plains Climate Research Facility." In Proceedings of the Sixteenth Atmospheric Radiation (ARM ) Science Team Meeting, Ed. by D Carrothers, U.S. Department of Energy, Richland, WA.

Ogawa K., and T. Schmugge, 2004: Mapping surface broadband emissivity of the Sahara Desert using ASTER andMODIS data," *Earth Interact.*, vol. 8, no. 7, pp. 1–14, May 2004. DOI: 10.1175/1087-3562.

Peres, L. F. and C. C. DaCamara, (2005): Emissivity maps to retrieve land-surface temperature from MSG/SEVIRI, *IEEE Trans. Geosci. Remote Sens.*, vol. 43, no. 8, pp. 1834–1844.

Rodgers, C.D., 1976: Retrieval of atmospheric temperature and composition from remote measurements of thermal radiation. *Rev. Geophys. Spac. Phys*., 14, 609-624.

Rodger, A. P., L. K. Balick, and W. B. Clodius, 2005: The performance of the Multispectral Thermal Imager (MTI) surface temperature retrieval algorithm at three sites," *IEEE Trans. Geosci. Remote Sens.*, vol. 43, no. 3, pp. 658–665.

Rothman, L. S., et al. (1992), The HITRAN molecular database: Editions of 1991 and 1992, J. Quant. Spectrosc. Radiat. Transfer, 48, 469–507, doi:10.1016/0022-4073(92)90115-K.

Salisbury, J. W., A. Wald, and D. M. D'Aria, 1994: Thermal-infrared remote sensing and Kirchhoff's law 1. Laboratory measurements. J. Geophys. Res., 99, 11 897–11 911.

Schmetz, J., P. Pili, S. Tjemkes, D. Just, J. Kerkman, S. Rota, and A. Ratier, 2002: An introduction toMeteosat Second Generation (MSG)," *Bull. Amer. Meteorol. Soc.*, vol. 83, no. 7, pp. 977–992.

Schmid J, 2000. The SEVIRI Instrument. Proceedings of the 2000 EUMETSAT Meteorological Satellite Data User's Conference, Bologna, Italy, 29 May – 2 June 2000

Schmit, T. J., M. M. Gunshor, W. Paul Menzel, J. Gurka, J. Li, and S. Bachmeier (2005), Introducing the next-generation advanced baseline imager (ABI) on GOES-R, Bull. Am. Meteorol. Soc., 86, 1079– 1096, doi:10.1175/BAMS-86-8-1079.

Schumann W, Stark H, McMullan K, Aminou D, Luhmann H-J. 2002. The MSG System, *ESA bulletin*, 111.

Seemann, S., E. Borbas, R. Knuteson, H.-L. Huang, and G. R. Stephenson, and H. – L. Huang (2008), Development of a global infrared land surface emissivity database for application to clear sky sounding retrievals from multispectral satellite radiance measurements, *J. Appl. Meteorol*., 47, 108 - 123.

Sherlock, V., 1999: *ISEM-6: Infrared Surface Emissivity Model for RTTOV-6*, EUMETSAT NWP SAF, 17 pp. [Online]. Available: http://www. metoffice.gov.uk/research/interproj/nwpsaf/rtm/rtm_reports.html

Snyder, W. C., Z. Wan, Y. Zhang, and Y.-Z. Feng, 1998: Classification-based emissivity for land surface temperature measurement from space," *Int. J. Remote Sens.*, vol. 19, no. 14, pp. 2753–2774.

Trigo, I. F. and P. Viterbo, 2003: Clear sky window channel radiances: A comparison between observations and the ECMWF model," *J. Appl. Meteorol.*, vol. 42, no. 10, pp. 1463–1479.

Turner, D. D., B. M. Lesht, S. A. Clough, J. C. Liljegren, H. E. Revercomb, and D. C. Tobin (2003), Dry bias and variability in Vaisala RS80-H radiosondes: The ARM experience, J. Atmos. Oceanic Technol., 20(1), 117 – 132.

Wan, Z., and J. Dozier (1996), A generalized split-window algorithm for retrieving land-surface temperature from space. *IEEE Transactions on Geosciences and Remote Sensing*, 34, 892-905.

Wan, Z., and Z.-L. Li (1997), A physics-based algorithm for retrieving land-surface emissivity and temperature from EOS/MODIS data, *IEEE Trans. Geosci. Remote Sens., 35*, 980-996.

Watson K., 1992: Two-temperature method for measuring emissivity, *Remote Sens. Environ.*, vol. 42, no. 2, pp. 117–121.

Yu, Y., J. L. Privette, and A. C. Pinheoro (2008), Evaluation of split window land surface temperature algorithms for generating climate data records, *IEEE Trans. Geosci. Remote Sens.*, 46, 179 - 192.

Zhang, P., N. Lu, X. Hu. and C. H. Dong (2006), Identification and physical retrieval of

dust storm using three MODIS thermal IR, *Global and Planetary Change*, 52, 197–206.

Zhou, L.; M. Goldberg, C. Barnet, Z. Cheng, F. Sun, W. Wolf, T. King, X. Liu, H. Sun, and M. Divakarla (2008), Regression of surface spectral emissivity from hyperspectral Instruments, *IEEE Trans. Geosci. Remote Sens.*, 46, 328-333.

# 8. APPENDIX

Table A1: LSE output variables – quality flags

| Variable Name | Unit | Type | Size† | Description |
|---|---|---|---|---|
| Quality_Flag | none | Int8 | NX_NY | Overall quality flag :<br>=0 : good<br>=1 : space<br>=2 : latitude greater than threshold<br>=3 : satellite zenith angle greater than threshold<br>=4 : number of clear pixels less than threshold<br>=5 : missing NWP data<br>=6 : fatal processing error |
| Quality_Flag_Rtvl | none | Int8 | NX_NY | Retrieval quality flag:<br>=0: good retrieval<br>=1: non-convergence<br>=2: residual too large<br>=3: non-completed converge<br>=4: bad retrieval |
| Quality_Flag_$K_{ts,12\,\mu m}$# | none | Int8 | NX_NY | Surface sensitivity quality:<br>=0: $K_{ts,12\,\mu m}$>0.3, good<br>=1: $K_{ts,12\,\mu m}$<=0.3 bad |

† NX_NY refers to the number of FORs in the x-direction by the number of FORs in the y-direction

#: $K_{ts,12\,\mu m}$ is the LST weighting function of 12 micron.

Table A2: LSE output variables -- quality information

| Variable Name | Unit | Type | Size† | Description |
|---|---|---|---|---|
| Num_Iteration | none | Int8 | NX_NY | Number of iterations |
| RMSE_BrtTemp_Next | K | Float32 | NX_NY | RMSE of average BT residual after retrieval |
| Num_Clr_Pix | none | Int8 | NX_NY | Number of clear pixels in FOR@ |

† NX_NY refers to the number of FORs in the x-direction by the number of FORs in the y-direction

@: this number changes with the FOR size.

Table A3: LSE meta-data

| Name | Details/Comments |
|---|---|
| | |
| Date | swath beginning and swath end |
| Time | swath beginning and swath end |
| Bounding Box | product resolution<br>number of rows and<br>number of columns,<br>bytes per pixel |

| | data type<br>byte order information<br>location of box relative to nadir (pixel space) |
|---|---|
| Product Name | |
| Product Units | |
| Ancillary Data to Produce Product | product precedence |
| Version Number | |
| Origin | where it was produced |
| Quality Information | |
| Name | |
| Satellite | GOES-16, etc. |
| Instrument | ABI |
| Altitude | |
| Nadir pixel in the fixed grid | |
| Attitude | |
| Latitude | |
| Longitude | |
| Grid Projection | |
| Type of Scan | |
| Product Version Number | |
| Data compression type | |
| Location of production | |
| Citations to Documents | |
| Contact Information | |
| | |
| For each LSE product, the following information is required: | |
| Mean, Min, Max and Standard deviation of retrievals from first guess | for LSE |
| Number of IR channels, channel 8 to channel 16 | |
| For each IR channel, the following information is required:<br>Mean difference between calculated BT (from first guess) and observed BT for the IR channel | |
| Number of QA flag values | |
| For each QA flag value, the following information is required:<br>Percent of retrievals with the QA flag value<br>Definition of QA flag | |
| Total number of attempted retrievals | |